

Sensing for Communication: RIS-Assisted ISAC Coordination Gain Enhancement With Imperfect CSI

Xiaohui Li, *Member, IEEE*, Qi Zhu, Yunpei Chen, Chadi Assi, *Fellow, IEEE*, Yifei Yuan, *Fellow, IEEE*

Abstract—Integrated sensing and communication (ISAC) has the potential to facilitate coordination gains from mutual assistance between sensing and communication (S&C), especially sensing-aided communication enhancement (SACE). Reconfigurable intelligent surface (RIS) is another potential technique for achieving resource-efficient communication enhancement. Therefore, this paper proposes an innovative RIS-assisted SACE (R-SACE) mechanism with the goal of improving the systemic communication performance of the ISAC system in practical scenarios where the channel status information (CSI) is imperfectly known. In the proposed R-SACE mechanism, a dual-functional base station (BS) provides downlink communication services to both the communication user and the dynamically changing target that is detected using the communication signals. RIS assists in both sensing and communications of the BS. A typical scenario is investigated in which either or both the direct and RIS-assisted reflected communication links are available depending on sensing results. The average systemic throughput (AST) over the entire timeline of the R-SACE mechanism is maximized by jointly optimizing both temporal and spatial resources under the probabilistic constraint and the sensing performance, transmission power, and communication interference constraints. The non-convex probabilistic mixed optimization problem is transformed and then solved by the proposed fixed-point iterative (FPI) algorithm. Simulation results demonstrate that the proposed FPI algorithm and R-SACE mechanism outperform the baseline algorithms and communication enhancement mechanisms in achieving higher systemic communication performance.

Index Terms—Integrated sensing and communication, reconfigurable intelligent surface, resource allocation, imperfect CSI

I. INTRODUCTION

INTEGRATED sensing and communication (ISAC) has been formally approved as one of key usage scenarios in

Xiaohui Li is with the School of Communication and Information Engineering, Nanjing University of Posts and Telecommunications, Nanjing, China, and also with the College of Electronic Information and Optical Engineering, Taiyuan University of Technology, Taiyuan, China (e-mail: lixiaohui@njupt.edu.cn)

Qi Zhu is with the School of Communication and Information Engineering, Nanjing University of Posts and Telecommunications, Nanjing 210003, China. (e-mails: zhuqi@njupt.edu.cn)

Yunpei Chen is with the School of Marine Information Engineering, Hainan Tropical Ocean University, Sanya 572022, China, with the School of Communication and Information Engineering, Nanjing University of Posts and Telecommunications, Nanjing 210003, China. (e-mail: 18913823955@189.cn)

Chadi Assi are with the Concordia Institute for Information Systems Engineering (CIISE), Concordia University, Montreal, QC H3G 1M8, Canada (email: chadi.assi@concordia.ca)

Yifei Yuan is with Future Mobile Technology Lab, China Mobile Research Institute, Beijing 100053, China (e-mail: yuanyifei@chinamobile.com).

(Corresponding author: Yunpei Chen.)

6G vision framework. Different from conventional separate sensing and communication systems, ISAC is capable of unifying sensing and communication (S&C) functionalities in a resource-efficient way by sharing hardware and wireless resources [1], [2]. ISAC has the potential to support both integration gain and coordination gain of S&C [3], [4]. The integration gain is for the dual purposes of S&C by sharing the congested wireless resources, while the coordination gain benefits from mutual assistance between S&C, allowing for communication-aided sensing enhancement (CASE) and sensing-aided communication enhancement (SACE) [5]. This paper focuses on improving the coordination gain, particularly the SACE, of ISAC systems.

Reconfigurable intelligent surface (RIS) is another promising technology in 6G for improving resource-efficient sensing and communication performances. In particular, RIS is typically a planar array with numerous low-cost and hardware-efficient passive reflecting elements installed. By designing the phase shift intelligently, RIS is capable of reshaping the radio propagation environment, particularly creating useful line-of-sight (LoS) links to support S&C [6]. Currently, there are four main types of RIS: passive RIS, active RIS [7], hybrid passive/active RIS [8], and simultaneously transmitting and reflecting RIS (STAR-RIS) [9]. In particular, active RIS deploys signal amplifiers into elements, which effectively overcomes severe channel fading. The hybrid RIS combines passive reflectors and active sensors, allowing it to reflect incident signals while also sensing essential information. When the transmitter and receiver are situated on opposite sides of the RIS, the STAR-RIS is more effective because it can simultaneously send and receive incident signals onto both sides of the space around the RIS. Among the four types of RIS designs, passive RIS has the following advantages in assisting the SACE mechanism. First, the passive RIS-assisted SACE method has the least hardware complexity in practice because it requires no extra hardware deployments. Second, the passive RIS-assisted SACE mechanism holds promise for facilitating more resource-efficient performance improvements in communication and sensing. Third, the passive RIS-assisted SACE mechanism has the potential to improve systemic communication performance because it does not amplify the thermal noise as additional communication interference. Lastly, the situation in which the transmitter and receiver are on the same side of the RIS is examined in this work. As a result, the passive RIS benefits SACE more than the STAR-RIS, particularly the energy splitting (ES) based STAR-RIS,

TABLE I
COMPARISON OF RELATED WORK ABOUT RIS-ASSISTED SACE

Related work	RIS structure	Communication scenario	Optimized Resource	Communication performance	CSI condition
[20]	Semi-passive	Blocked BS-user link	BS Beamforming and RIS phase shift	Received signal power at BS	Acquiring user location information instead of CSI
[21]	Passive and semi-passive			Sum rate of users	
[22]	Passive		RIS phase shift	Achievable data rate of a user	Acquiring user orientation instead of CSI
[23]			Time and RIS phase shift	Average achievable capacity of a user	Perfect CSI
[24]		Available BS-user link or BS-RIS-user link			
Proposed		Available BS-RIS-user link and probabilistic available direct link	Time, BS beamforming, and RIS phase shift	Average systemic throughput	Imperfect CSI

because all of the energy can be used to reflect incident signals toward the desired side of the RIS.

The benefits of RIS have attracted lots of research interests in incorporating RIS into ISAC to improve the integration and coordination gains.

A. Related Works and Motivations

Numerous efforts [10]–[18] have studied the RIS-assisted integration gain improvement for ISAC systems. In the integration-gain-oriented ISAC systems, the effective wireless resource sharing between S&C is investigated for maximizing the communication performance [10]–[13] or the sensing performance [14]–[18] under constraints of sensing or communication performances. Nonetheless, mutual assistance between S&C, such as the aids of sensing results in facilitating communication, is rarely involved in integration-gain-oriented ISAC systems, despite its significance for enhancing coordination gain of ISAC systems. Specifically, S&C in the coordination-gain-oriented ISAC system are not only coupled in wireless resources, as in integration-gain-oriented ISAC systems, but also interdependent in their functions. As a result, the research on integration-gain-oriented ISAC systems can not be directly applied into the coordination-gain-oriented ISAC systems. Especially as sensing begins to rise as a fundamental service in ISAC [5], it's necessary to investigate the SACE mechanism for improving ISAC coordination gains. Moreover, taking advantage of RIS in establishing controllable supplementary links, the RIS-assisted SACE mechanism could provide extra sensing degrees of freedom while suppressing co-channel communication interference, allowing for enhanced communication performance with the help of desirable sensing results. Therefore, the study on RIS-assisted SACE mechanisms, which involves S&C couplings in both wireless resource and functional assistance, is crucially important and meaningful for ISAC coordination gain enhancement, which motivates the research in our paper.

To the best of our knowledge, a limited number of works [20]–[24] have begun to investigate the RIS-assisted SACE for improving ISAC coordination gain. The S&C in a coordination-gain-oriented ISAC system are mutually constrained by limited wireless resources and mutually helpful, especially in a SACE system where communication signals

support sensing and sensing results help facilitate communication further. RIS in SACE is to assist in sensing or sensing-aided communication. The goal of RIS-assisted SACE is maximizing the communication performance with aids of RIS and performance-guaranteed sensing results.

A summary of the related work about RIS-assisted SACE is shown in Table I. Specifically, in [20], a sub-passive RIS helps uplink communication while also estimating user location in each time unit using the communication signal. The estimated user location helps with the precoding design of RIS in the next time unit. In [21], authors extend [20] by using passive and sub-passive RIS for location estimations and uplink communications of multiple users. The sum rate is maximized by jointly optimizing the beamforming and the phase shift of RIS using estimated user locations. In [22], the ISAC frame structure consists of a sensing time unit and a communication time unit. During the sensing unit, the RIS helps estimate the angle of departure (AoD) of the communication user. Then, based on the obtained AoD, the RIS assists in modifying the transmission signal of the base station (BS) during the communication unit. The spatial codebook of the RIS is optimized to enhance sensing accuracy and improve the achievable rate. In summary, the authors in [20]–[22] use sensed user location information to replace the acquisition of CSI to facilitate communication. The spatial resource, including beamforming and phase shift, is optimized in [20]–[22]. The optimization of temporal resources, such as time allocation among different time units, remains to be investigated further. In [23] and [24], the BS communicates with a legacy receiver and simultaneously detects a target in each time unit. Based on the sensing result and RIS assistance, the downlink communication links, which include the direct and RIS-assisted reflected links, are optimally designed in the subsequent time unit. The average achievable capacity of the receiver is maximized by jointly optimizing the phase shift of RIS and the time allocation between two time units. The authors in [23] and [24] assume perfect CSI for evaluating the upper bond of communication performance.

The above works lay important groundwork for improving ISAC communication performance with assistance of sensing and RIS. These works improve the ISAC communication performance based on either the perfect channel status infor-

model of the proposed R-SACE mechanism consists of a dual-functional ISAC BS with K transmitting and K sensing antennas, a static communication user CU I , a dynamic target TC J , and a RIS equipped with N_R elements. The CU I is a pure communication user who receives communication signals from the BS throughout the timeline. The TC J is an aperiodically present device-based target that needs to be detected and also a communication terminal that has communication requirements. The TC J could be a person, vehicle, or drone that takes communication equipments [5] in practice¹. Thus, when TC J is present and correctly detected by the BS, TC J also emerges as a potential communication user of the BS. This is different from [11], [12], [16], [17], [21], where the target has no communication needs but only to be detected. RIS assists in both sensing and communication in the proposed R-SACE mechanism. Specifically, RIS helps BS detect TC J and reconstruct another feasible communication link that facilitates the downlink communication while suppressing mutual interference².

The time protocol of the proposed R-SACE model is illustrated in Fig. 2. The entire timeline with τ time slots includes an ISAC period with τ_1 time slots and a pure communication (PC) period with $\tau - \tau_1$ time slots. During the ISAC period, the BS communicates with CU I through both direct BS-CU I link and the RIS-assisted BS-RIS-CU I link and meanwhile detects TC J using the communication signal. During the PC period, the BS performs downlink communications with assistance of RIS and based on the sensing result obtained at the ISAC period. Specially, when BS detects TC J being present, it communicates with CU I through the RIS-assisted BS-RIS-CU I link and meanwhile communicates with TC J through the direct BS-TC J link. Additionally, when BS detects TC J being absent, it communicates with CU I through both the direct BS-CU I link and the BS-RIS-CU I link.

We use a and d to indicate the actual and detected statuses of TC J , respectively. Specially, $a = 1$ (or $a = 0$) indicates that the TC J is actually present (or absent). $d = 1$ (or $d = 0$) indicates that the BS detects TC J being present (or absent).

A. Sensing Model

During ISAC period, the BS transmits the signal s_1 to CU I and simultaneously uses s_1 to detect TC J with assistance of RIS [26]. As shown in Fig. 1, when TC J is truly present, the signal s_1 is reflected back to the BS from both TC J and

¹As a potential scenario, TC J can be a manoeuvrable UAV that provides emergency communication supports for users in challenging environments, such as earthquake areas, that cannot be directly served by the BS. Under this scenario, the TC J dynamically supports a variety of emergence areas. Consequently, it is necessary to detect TC J as it is not a fixed authorized communication user of the BS. When TC J is present and correctly detected by the BS, it provides communication supports by acting as a communication relay between the BS and the CU I .

²Note that the proposed R-SACE mechanism is an orthogonal multiple access (OMA) system, which is different from the rate splitting multiple access (RSMA) and non-orthogonal multiple access (NOMA) in terms of interference management. In particular, the main contribution of the proposed R-SACE mechanism is utilizing sensing and the RIS-assisted reconstructed link to coordinate mutual interference. This is different from NOMA and RSMA mechanisms in which power allocation and successive interference cancellation are typically adopted to manage interference.

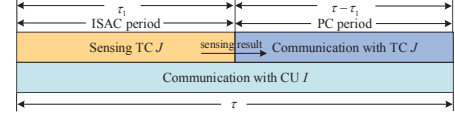


Fig. 2. Illustration of the time protocol of the proposed R-SACE mechanism.

RIS. As a result, the echo signal received at the BS at time slot $\forall t \in \{1, \dots, \tau_1\}$ can be given by [25], [26]

$$\mathbf{z}_B(t) = a(\mathbf{G}^H \mathbf{\Lambda} \mathbf{A} \mathbf{A} \mathbf{G} + \mathbf{B}) \mathbf{w}_0 s_1(t) + \mathbf{n}_B, \quad (1)$$

where $\mathbb{E}[|s_1|^2] = 1$. $\mathbf{G} \in \mathbb{C}^{N_R \times K}$ represents the channel between BS and RIS. $\mathbf{\Lambda} \in \mathbb{C}^{N_R \times N_R}$ represents the phase shift matrix of RIS at the ISAC period. $\mathbf{A} = \alpha_A \mathbf{a}_{Ar}(\theta_A) \mathbf{a}_{At}^H(\theta_A)$ and $\mathbf{B} = \alpha_B \mathbf{a}_{Br}(\theta_B) \mathbf{a}_{Bt}^H(\theta_B)$ represent the response matrices [25], [26] of RIS and BS, respectively. α_A and α_B denote the reflection coefficients incorporating effects of radar cross section (RCS) $\alpha_T \sim (0, \sigma_T^2)$ and path losses of RIS-TC J and BS-TC J links, respectively [11], [25]. θ_A and θ_B represent the direct-of-arrivals (DoAs) of the target with respect to RIS and BS. \mathbf{a}_{At} , \mathbf{a}_{Bt} and \mathbf{a}_{Ar} , \mathbf{a}_{Br} represent the transmit and receive steering vectors at RIS and BS, respectively. In particular, $\mathbf{a}_{At} = [1, e^{-j\pi \sin \theta_A}, \dots, e^{-j(N_R-1)\pi \sin \theta_A}]^T$ and $\mathbf{a}_{Bt} = [1, e^{-j\pi \sin \theta_B}, \dots, e^{-j(K-1)\pi \sin \theta_B}]^T$. \mathbf{a}_{Ar} and \mathbf{a}_{Br} can be similarly expressed based on \mathbf{a}_{At} and \mathbf{a}_{Bt} , respectively. $\mathbf{w}_0 \in \mathbb{C}^{K \times 1}$ is the beamforming vector of s_1 . \mathbf{n}_B represents the CSCG noise at the BS, with $\mathbf{n}_B \sim \mathcal{CN}(\mathbf{0}_K, \mathbf{1}_K \sigma_0^2)$.

Then, the BS samples the received $\mathbf{z}_B(t)$ over the duration of τ_1 with a sampling frequency of f_s , thereby conducting a hypothesis test statistic T_e . Following the chi-square distribution of T_e and central limit theorem (CLT) [5], [13], [24], [28], the sensing performance including detection probability P_d and false alarm probability P_f obtained at the BS can be given respectively by

$$P_d = \Pr(T_e > \epsilon | a = 1) = Q\left(\sqrt{\tau_1} f_s \left(\frac{\epsilon}{\|(\mathbf{G}^H \mathbf{\Lambda} \mathbf{A} \mathbf{A} \mathbf{G} + \mathbf{B}) \mathbf{w}_1\|^2 + \|\mathbf{n}_B\|^2} - 1 \right)\right), \quad (2)$$

$$P_f = \Pr(T_e > \epsilon | a = 0) = Q\left(\sqrt{\tau_1} f_s \left(\frac{\epsilon}{\|\mathbf{n}_B\|^2} - 1 \right)\right) \quad (3)$$

where $Q(x) = \frac{1}{\sqrt{2\pi}} \int_x^\infty \exp(-\frac{t^2}{2}) dt$, ϵ is the detection threshold. To be specific, P_f represents the probability of that BS wrongly detects the presence of TC J when TC J is truly absent. P_d represents the probability of that BS correctly detects the presence of TC J . Let P_{J_1} and $P_{J_0} = 1 - P_{J_1}$ denote the probabilities of TC J being actually present or absent, respectively. There exist four potential cases with corresponding probabilities as follows:

- *Case 1:* When TC J is truly present and is correctly detected by the BS, i.e., $a = 1$ and $d = 1$, the corresponding probability is $P_{11} = \Pr(a = 1, d = 1) = P_d P_{J_1}$.
- *Case 2:* When TC J is truly present but not correctly detected by the BS, i.e., $a = 1$ and $d = 0$, the corresponding probability is $P_{10} = \Pr(a = 1, d = 0) = (1 - P_d) P_{J_1}$.
- *Case 3:* When TC J is truly absent and is correctly detected by the BS, i.e., $a = 0$ and $d = 0$, the corresponding probability is $P_{00} = \Pr(a = 0, d = 0) = (1 - P_f) P_{J_0}$.

- *Case 4:* When TC J is truly absent but detected as present by the BS, i.e., $a = 0$ and $d = 1$, the corresponding probability is $P_{01} = \Pr(a = 0, d = 1) = P_f P_{J_0}$.

B. Communication Model

1) *ISAC period:* During the ISAC period, the BS communicates with CU I through both the direct BS-CU I link and the RIS-assisted BS-RIS-CU I link. Therefore, the signal received at the CU I at time slot $t \in \{1, \dots, \tau_1\}$ can be given by

$$Z_{I(1)}(t) = (\mathbf{g}_{RI}^H \mathbf{\Lambda} \mathbf{G} + \mathbf{h}_I^H) \mathbf{w}_0 s_1(t) + n_I, \quad (4)$$

where $\mathbf{g}_{RI} \in \mathbb{C}^{N_R \times 1}$ represents the channel between RIS and CU I , $\mathbf{h}_I \in \mathbb{C}^{K \times 1}$ represents the channel between BS and CU I , $n_I \sim \mathcal{CN}(0, \sigma_I^2)$ is the receiver noise at the CU I .

2) *PC period:* During the PC period, the BS communicates with CU I and TC J based on the sensing result and with assistance of RIS. To be specific, when the BS detects the TC J being present, i.e., $d = 1$, it transmits signals s_1 and s_2 to CU I and TC J , respectively. The RIS-assisted BS-RIS-CU I link is used for the communication of CU I while the direct BS-TC J link is used for the communication of TC J . On the other side, when BS detects the TC J being absent, i.e., $d = 0$, it transmits s_1 to CU I through the direct BS-CU I link and the RIS-assisted BS-RIS-CU I link.

As a result, the signal received at CU I at time slot $t \in \{1, \dots, \tau - \tau_1\}$ can be given by

$$Z_{I(2)}^{(d)}(t) = (\mathbf{g}_{RI}^H \mathbf{\Theta} \mathbf{G} + (1-d)\mathbf{h}_I^H) \mathbf{w}_I s_1(t) + d\mathbf{h}_I^H \mathbf{w}_J s_2(t) + n_I \quad (5)$$

where \mathbf{w}_I and \mathbf{w}_J represents the beamforming vectors of s_1 and s_2 , respectively; $\mathbf{\Theta} \in \mathbb{C}^{N_R \times N_R}$ is the phase shift matrix of RIS³. The first term in $Z_{I(2)}^{(d)}(t)$ represents the desired signal received at CU I from the BS-RIS-CU I link and the direct BS-CU I link (i.e., when $d = 0$). The second term in $Z_{I(2)}^{(d)}(t)$ represents the interference experienced by CU I from s_2 when BS detects the TC J being present (i.e., when $d = 1$).

Additionally, the signal received at the truly present TC J at time slot $t \in \{1, \dots, \tau - \tau_1\}$ can be given by

$$Z_J^{(d)}(t) = d\mathbf{h}_J^H \mathbf{w}_J s_2(t) + \mathbf{g}_{RJ}^H \mathbf{\Theta} \mathbf{G} \mathbf{w}_I s_1(t) + n_J, \quad (6)$$

where $\mathbf{h}_J \in \mathbb{C}^{K \times 1}$ represents the channel between BS and TC J , $\mathbf{g}_{RJ} \in \mathbb{C}^{N_R \times 1}$ represents the channel between RIS and TC J . The first term in $Z_J^{(d)}(t)$ is the desired signal received at the present TC J when it is correctly detected by BS (i.e., when $d = 1$). The second term in $Z_J^{(d)}(t)$ is the interference experienced by the present TC J . $n_J \sim \mathcal{CN}(0, \sigma_J^2)$ represents the CSCG noise at the TC J .

³Note that \mathbf{w}_I and $\mathbf{\Theta}$ in the PC period are different from \mathbf{w}_0 and $\mathbf{\Lambda}$ in the ISAC period, since BS communicates with both CU I and TC J in the PC period. Therefore, \mathbf{w}_I , \mathbf{w}_J , and $\mathbf{\Theta}$ need to be optimally designed in the PC period for restricting mutual interference and ultimately facilitating the systemic communication enhancement.

C. Systemic Communication Performance With Imperfect CSI

In practice, it is hard to obtain the CSI of \mathbf{h}_I and \mathbf{h}_J perfectly⁴. Therefore, the systemic communication performance with imperfect CSI is worthwhile to explore in this paper.

We assume $\mathbf{h}_I = L_I \mathbf{f}_I$ and $\mathbf{h}_J = L_J \mathbf{f}_J$, where $\mathbf{f}_I \sim \mathcal{CN}(\mathbf{0}_K, \mathbf{1}_K)$ and $\mathbf{f}_J \sim \mathcal{CN}(\mathbf{0}_K, \mathbf{1}_K)$. Generally, the small-scale Rayleigh fading coefficients \mathbf{f}_I and \mathbf{f}_J have server effects on the channel estimation accuracy than the large-scale pass loss coefficients L_I and L_J . Therefore, according to the minimum mean square error channel estimation error model [31]–[33], \mathbf{h}_I and \mathbf{h}_J can be rewritten as

$$\mathbf{h}_I = L_I \mathbf{f}_I = L_I (\hat{\mathbf{f}}_I + \mathbf{e}_I) \quad (7)$$

$$\mathbf{h}_J = L_J \mathbf{f}_J = L_J (\hat{\mathbf{f}}_J + \mathbf{e}_J) \quad (8)$$

respectively. \mathbf{e}_I and \mathbf{e}_J denote the estimation error vectors in which each element follows complex Gaussian distribution with mean zero and variance σ_e^2 . $\hat{\mathbf{f}}_I$ and $\hat{\mathbf{f}}_J$ denote the estimated Rayleigh fading coefficients that follow $\mathcal{CN}(\mathbf{0}_K, \mathbf{1}_K(1 - \sigma_e^2))$.

Then, according to Eqs. (4)–(8), the data rates of CU I and TC J obtained with imperfect CSI during the ISAC period and the PC period can be given as

$$\hat{R}_l = \begin{cases} \hat{R}_{I(1)} = \log_2(1 + \hat{\gamma}_{I(1)}) = \log_2(1 + \hat{\gamma}_0), & l = 0, \\ \hat{R}_{I(2)}^{(1)} = \log_2(1 + \hat{\gamma}_{I(2)}^{(1)}) = \log_2(1 + \hat{\gamma}_1), & l = 1, \\ \hat{R}_{I(2)}^{(0)} = \log_2(1 + \hat{\gamma}_{I(2)}^{(0)}) = \log_2(1 + \hat{\gamma}_2), & l = 2, \\ \hat{R}_J^{(1)} = \log_2(1 + \hat{\gamma}_J^{(1)}) = \log_2(1 + \hat{\gamma}_3), & l = 3, \end{cases} \quad (9)$$

where the signal-to-interference-and-noise ratio (SINR) $\gamma_l, \forall l$ is obtained as

$$\hat{\gamma}_l = \begin{cases} \hat{\gamma}_{I(1)} = \frac{|\mathbf{g}_{RI}^H \mathbf{\Lambda} \mathbf{G} \mathbf{w}_0 + \hat{\mathbf{h}}_I^H \mathbf{w}_0|^2 / \sigma_I^2}{= (|\mathbf{g}_{RI}^H \mathbf{\Lambda} \mathbf{G} \mathbf{w}_0|^2 + L_I^2(1 - \sigma_e^2) |\mathbf{1}_K^H \mathbf{w}_0|^2) / \sigma_I^2}, & l = 0, \\ \hat{\gamma}_{I(2)}^{(1)} = \frac{|\mathbf{g}_{RI}^H \mathbf{\Theta} \mathbf{G} \mathbf{w}_I|^2 / (|\hat{\mathbf{h}}_I^H \mathbf{w}_J|^2 + \sigma_I^2)}{= |\mathbf{g}_{RI}^H \mathbf{\Theta} \mathbf{G} \mathbf{w}_I|^2 / (L_I^2(1 - \sigma_e^2) |\mathbf{1}_K^H \mathbf{w}_J|^2 + \sigma_I^2)}, & l = 1, \\ \hat{\gamma}_{I(2)}^{(0)} = \frac{|\mathbf{g}_{RI}^H \mathbf{\Theta} \mathbf{G} \mathbf{w}_I + \hat{\mathbf{h}}_I^H \mathbf{w}_I|^2 / \sigma_I^2}{= (|\mathbf{g}_{RI}^H \mathbf{\Theta} \mathbf{G} \mathbf{w}_I|^2 + L_I^2(1 - \sigma_e^2) |\mathbf{1}_K^H \mathbf{w}_I|^2) / \sigma_I^2}, & l = 2, \\ \hat{\gamma}_J^{(1)} = \frac{|\hat{\mathbf{h}}_J^H \mathbf{w}_J|^2 / (|\mathbf{g}_{RJ}^H \mathbf{\Theta} \mathbf{G} \mathbf{w}_I|^2 + \sigma_J^2)}{= L_J^2(1 - \sigma_e^2) |\mathbf{1}_K^H \mathbf{w}_I|^2 / (|\mathbf{g}_{RJ}^H \mathbf{\Theta} \mathbf{G} \mathbf{w}_I|^2 + \sigma_J^2)}. & l = 3, \end{cases} \quad (10)$$

where $\hat{\mathbf{h}}_I = L_I \hat{\mathbf{f}}_I$ and $\hat{\mathbf{h}}_J = L_J \hat{\mathbf{f}}_J$. In particular, $l = 0$ represents the communication scenario during ISAC period where BS communicates with CU I ; $l = 1$ represents the

⁴This paper primarily studies the imperfect CSI of direct links \mathbf{h}_I and \mathbf{h}_J . The estimation of cascaded channels $\mathbf{g}_{RI}^H \mathbf{\Lambda} \mathbf{G}$, $\mathbf{g}_{RI}^H \mathbf{\Theta} \mathbf{G}$ and $\mathbf{g}_{RJ}^H \mathbf{\Theta} \mathbf{G}$ in RIS-assisted systems is a more challenging task that can be addressed by effective methods, such as the joint bilinear factorization and matrix completion method [29] and the progressive channel estimation method [30]. For instance, let $\mathbf{g}_{RI} = \text{diag}(\mathbf{g}_{RI}^H) \mathbf{G}$ and $Z_{I(2)}^{(d)}(t) = \mathbf{g}_{RI}^H \mathbf{\Theta} \mathbf{G} \mathbf{w}_I s_1(t)$ in Eq. (5). Then, the least-square (LS) estimation model [30] of \mathbf{g}_{RI}^H can be given as $\hat{\mathbf{g}}_{RI}^H = (\mathbf{w}_I s_1(t))^{-1} \boldsymbol{\theta}^{-1} Z_{I(2)}^{(d)}(t) = \mathbf{g}_{RI}^H + \mathbf{e}_{RI}$, where $\boldsymbol{\theta}$ is the diagonal vector of $\mathbf{\Theta}$; $\mathbf{e}_{RI} = (\mathbf{w}_I s_1(t))^{-1} \boldsymbol{\theta}^{-1} \Delta$ is the channel estimation error, and $\Delta = Z_{I(2)}^{(d)}(t) - Z_{I(2)}^{(d)}(t)$. Then, the mean-square error (MSE) $\mathbb{E}[\|\mathbf{g}_{RI}^H - \hat{\mathbf{g}}_{RI}^H\|^2]$ can be minimized by designing $\mathbf{\Theta}$ as referred to [30].

communication scenario during PC period where BS communicates with CU I when it detects TC J being present; $l = 2$ represents the communication scenario during PC period where BS communicates with CU I when it detects TC J being absent ; $l = 3$ represents the communication scenario during PC period where BS communicates with the TC J who is actually present and is correctly detected. We observe that the effects of CSI estimation errors σ_e^2 on communication performances vary from users and transmission periods. Especially for $\hat{\gamma}_{I(2)}^{(1)}$, the estimation error σ_e^2 affects the interference link rather than the signal links as in $\hat{\gamma}_{I(1)}$, $\hat{\gamma}_{I(2)}^{(0)}$, and $\hat{\gamma}_J^{(1)}$. The reason is that when BS detects TC J being present and then transmits s_2 to TC J , the CU I inevitably experiences interference from s_2 through the direct BS-CU I link. Therefore, the CSI estimation error σ_e^2 of \mathbf{h}_I effects the interference experienced by CU I when $d = 1$ during the PC period. Following Eq. (10), the probability of $\hat{R}_l, l \in \{1, 2, 3\}$

$$\text{is calculated as } P_l = \begin{cases} P_{I(2)}^{(1)} = P_{11} + P_{01}, & l = 1, \\ P_{I(2)}^{(0)} = P_{10} + P_{00} & l = 2, \\ P_J^{(1)} = P_{11}, & l = 3. \end{cases}$$

It's worth mentioning that data rates obtained with imperfect CSI may exceed achievable data rates obtained with perfect CSI due to estimation errors. Therefore, to address this issue, as referred to [33], we use average systemic throughput (AST) to evaluate the systemic communication performance of the proposed R-SACE mechanism obtained with imperfect CSI during the entire timeline. The AST can be calculated as

$$O_T = \frac{\tau_1}{\tau} \hat{R}_0 \Pr[\hat{R}_0 \leq R_0 | \hat{\mathbf{f}}_0] + \frac{\tau - \tau_1}{\tau} \sum_{l=1}^3 \hat{R}_l P_l \Pr[\hat{R}_l \leq R_l | \hat{\mathbf{f}}_l] \quad (11)$$

where $\Pr[\hat{R}_l \leq R_l | \hat{\mathbf{f}}_l], \forall l$ represent the probability that the data rate obtained with imperfect CSI deso not exceed the achievable data rate obtained with perfect CSI in each commu-

$$\text{nication case. } \hat{\mathbf{f}}_0 = \hat{\mathbf{f}}_1 = \hat{\mathbf{f}}_2 = \hat{\mathbf{f}}_I, \hat{\mathbf{f}}_3 = \hat{\mathbf{f}}_J. R_l = \begin{cases} R_{I(1)}, & l = 0, \\ R_{I(2)}^{(1)}, & l = 1, \\ R_{I(2)}^{(0)}, & l = 2, \\ R_J^{(1)}, & l = 3, \end{cases}$$

is the achievable data rate obtained with perfect CSI. We notice that the sensing performance, i.e., P_l , obtained at the ISAC period takes important impacts on the average systemic throughput obtained at the PC period, i.e., the second term in Eq. (11). Particularly, the communication performance of TC J is guaranteed only when the BS correctly detects the present TC J . Therefore, the detection accuracy should be improved through effective methods, such as the adaptive threshold method [39] or increasing sensing time τ_1 , i.e., the duration of ISAC period. Nevertheless, the increased τ_1 causes the decreased duration of PC period, which thus degrades the communication performance at the PC period and consequently degrades the AST during the entire timeline. As a result, the S&C balance in time allocation is a crucial issue for maximizing AST of the proposed R-SACE mechanism, which will be addressed in detail in the following section.

III. PROBLEM STATEMENT AND TRANSFORMATION

A. Problem Statement

The goal of this paper is to maximize the systemic communication performance with imperfect CIS in the proposed R-SACE mechanism with assistance of RIS and the performance-guaranteed sensing result obtained in the ISAC period. To be specific, we aim to maximize the AST O_T by jointly optimizing the time allocation τ_1 , the reflecting precoding Θ of RIS, and the downlink beamforming vectors \mathbf{w}_I and \mathbf{w}_J of the BS, under the probabilistic constraint and the sensing performance, transmission power, and communication interference constraints. In a word, the AST maximization problem can be formulated as

$$\begin{aligned} (\mathbf{P1}): \quad & \max_{\tau_1, \Theta, \mathbf{w}_I, \mathbf{w}_J} O_T \quad (12) \\ \text{s.t.} \quad & C1: \Pr[R_l < \hat{R}_l | \hat{\mathbf{f}}_l] \leq \epsilon_{\text{out}}, \forall l \\ & C2: P_d(\tau_1) \geq \bar{P}_d \\ & C3: P_f(\tau_1) \leq \bar{P}_f \\ & C4: \|\mathbf{w}_I\|^2 \leq p_{I\text{max}} \\ & C5: \|\mathbf{w}_J\|^2 \leq p_{J\text{max}} \\ & C6: |\mathbf{g}_{RJ}^H \Theta \mathbf{G} \mathbf{w}_I|^2 \leq \bar{\epsilon}_J \\ & C7: 0 < \tau_1 \leq \tau, \end{aligned}$$

where ϵ_{out} is the probability threshold; $\bar{\epsilon}_J$ is the threshold of the tolerable interference of TC J . $p_{I\text{max}}$ and $p_{J\text{max}}$ represent the maximum transmission power of the BS. \bar{P}_d and \bar{P}_f represent the thresholds of detection probability and false alarm probability, respectively. In $\mathbf{P1}$, $C1$ restricts the probability that the data rates obtained with imperfect CSI exceed the achievable data rates to less than ϵ_{out} . $C2$ and $C3$ guarantee the sensing performance. $C4$ and $C5$ are transmission power limit constraints. $C6$ is the interference constraint and $C7$ gives the available region of τ_1 .

For solving the non-convex probabilistic mixed problem effectively, we first transform $\mathbf{P1}$ into a non-probabilistic optimization problem by incorporating the probabilistic constraint $C1$ into the objective function.

B. Problem Transformation

We first rewrite $\hat{R}_l = \log_2(1 + \hat{\gamma}_l) = \log_2(1 + \frac{\hat{c}_l}{\hat{d}_l})$ and $R_l = \log_2(1 + \gamma_l) = \log_2(1 + \frac{c_l}{d_l})$. Then, according to the total probability theorem [33], the constraint $C1$ in Eq. (12) can be recast as

$$\begin{aligned} \Pr[\gamma_l < \hat{\gamma}_l | \hat{\mathbf{f}}_l] &= \Pr\left[\frac{c_l}{d_l} < \frac{\hat{c}_l}{\hat{d}_l} | \hat{\mathbf{f}}_l\right] \\ &= \Pr\left[\frac{c_l}{d_l} < 2^{\hat{R}_l} - 1 | c_l \leq \hat{c}_l, \hat{\mathbf{f}}_l\right] \cdot \Pr[c_l \leq \hat{c}_l | \hat{\mathbf{f}}_l] \\ &\quad + \Pr\left[\frac{c_l}{d_l} < 2^{\hat{R}_l} - 1 | c_l > \hat{c}_l, \hat{\mathbf{f}}_l\right] \cdot \Pr[c_l > \hat{c}_l | \hat{\mathbf{f}}_l] \\ &\leq \epsilon_{\text{out}} \end{aligned} \quad (13)$$

Proposition 1: Following [31]–[33], the constraint $C1$ can be further derived from the following two equations

$$\Pr[d_l \geq \hat{d}_l | \hat{\mathbf{f}}_l] \leq \epsilon_{\text{out}}/2 \quad (14)$$

$$\Pr \left[c_l \leq \hat{c}_l | \hat{\mathbf{f}}_l \right] = \epsilon_{\text{out}}/2. \quad (15)$$

Proof: Please refer to Appendix A. ■

Then, we integrate the probabilistic constraints in Eqs. (14) and (15) into the objective function O_T of the problem **P1**.

We first analyze the Eq. (14). Based on Eq. (10), we know that $\hat{d}_0 = \hat{d}_0 = \sigma_I^2$, $d_1 = |\mathbf{h}_I^H \mathbf{w}_J|^2 + \sigma_I^2$, $\hat{d}_1 = |\hat{\mathbf{h}}_I^H \mathbf{w}_J|^2 + \sigma_I^2$, $d_2 = \hat{d}_2 = \sigma_I^2$, $d_3 = \hat{d}_3 = |\mathbf{g}_{Rl}^H \Theta \mathbf{G} \mathbf{w}_J|^2 + \sigma_J^2$. Therefore, we only need to analyze $\Pr \left[d_1 \geq \hat{d}_1 | \hat{\mathbf{f}}_1 \right] \leq \epsilon_{\text{out}}/2$. By utilizing the Markov inequality theorem [32], [33], we have

$$\begin{aligned} \Pr \left[d_1 \geq \hat{d}_1 | \hat{\mathbf{f}}_1 \right] &= \Pr \left[|\mathbf{h}_I^H \mathbf{w}_J|^2 \geq (\hat{d}_1 - \sigma_I^2) | \hat{\mathbf{f}}_1 \right] \\ &\leq \frac{\mathbb{E} \left[|\mathbf{h}_I^H \mathbf{w}_J|^2 \right]}{\hat{d}_1 - \sigma_I^2} \leq \frac{\mathbb{E} \left[\|\mathbf{h}_I\|^2 \|\mathbf{w}_J\|^2 \right]}{\hat{d}_1 - \sigma_I^2} \quad (16) \\ &= \frac{L_I^2 \|\mathbf{f}_I\|^2 \|\mathbf{w}_J\|^2}{\hat{d}_1 - \sigma_I^2}. \end{aligned}$$

Based on $\hat{\gamma}_1 = \frac{\hat{c}_1}{\hat{d}_1}$, we substitute $\hat{d}_1 = \hat{c}_1/\hat{\gamma}_1$ and Eq. (16) into Eq. (14) and then we have

$$\frac{L_I^2 \|\mathbf{f}_I\|^2 \|\mathbf{w}_J\|^2}{\hat{d}_1 - \sigma_I^2} = \frac{L_I^2 (\|\hat{\mathbf{f}}_I\|^2 + \|\mathbf{1}\|^2 \sigma_e^2) \|\mathbf{w}_J\|^2}{\hat{c}_1/\hat{\gamma}_1 - \sigma_I^2} = \frac{\epsilon_{\text{out}}}{2}. \quad (17)$$

According to Eq. (17), we get the transformed expression $\tilde{\gamma}_1$ of $\hat{\gamma}_1$ as

$$\tilde{\gamma}_1 \triangleq \hat{\gamma}_1 = \frac{\epsilon_{\text{out}} \hat{c}_1}{2L_I^2 (\|\hat{\mathbf{f}}_I\|^2 + \|\mathbf{1}_K\|^2 \sigma_e^2) \|\mathbf{w}_J\|^2 + \epsilon_{\text{out}} \sigma_I^2}, \quad (18)$$

where $\hat{c}_1 = c_1 = |\mathbf{g}_{Rl}^H \Theta \mathbf{G} \mathbf{w}_J|^2$.

Next, we analyze Eq. (15). Considering $c_l = \hat{c}_l$, we only need to analyze $\Pr [c_l \leq \hat{c}_l | \hat{\mathbf{f}}_l, l = 0, 2, 3] = \epsilon_{\text{out}}/2$. According to Eq. (10), we have

$$\Pr \left[c_l \leq \hat{c}_l | \hat{\mathbf{f}}_l, l = 3 \right] = \Pr \left[|\mathbf{h}_J^H \mathbf{w}_J|^2 \leq \hat{c}_3 | \hat{\mathbf{f}}_J \right] = \epsilon_{\text{out}}/2, \quad (19)$$

and

$$\begin{aligned} &\Pr \left[c_l \leq \hat{c}_l | \hat{\mathbf{f}}_l, l = 0, 2 \right] \\ &= \Pr \left[|\mathbf{h}_l^H \mathbf{w}_l|^2 \leq (\hat{c}_l - A_l) | \hat{\mathbf{f}}_l, l = 0, 2 \right] = \epsilon_{\text{out}}/2, \quad (20) \end{aligned}$$

where $|\mathbf{h}_0^H \mathbf{w}_0|^2 = |\mathbf{h}_1^H \mathbf{w}_0|^2$, $|\mathbf{h}_2^H \mathbf{w}_2|^2 = |\mathbf{h}_I^H \mathbf{w}_I|^2$, $A_0 = |\mathbf{g}_{Rl}^H \Lambda \mathbf{G} \mathbf{w}_0|^2$, $A_2 = |\mathbf{g}_{Rl}^H \Theta \mathbf{G} \mathbf{w}_J|^2$. Since $|\mathbf{h}_l^H \mathbf{w}_l|^2 \leq \|\mathbf{h}_l\|^2 \|\mathbf{w}_l\|^2$ and $|\mathbf{h}_J^H \mathbf{w}_J|^2 \leq \|\mathbf{h}_J\|^2 \|\mathbf{w}_J\|^2$, Eq. (19) and Eq. (20) can be respectively refined as

$$\Pr \left[\|\mathbf{h}_J\|^2 \|\mathbf{w}_J\|^2 \leq \hat{c}_3 | \hat{\mathbf{f}}_J \right] = \Pr \left[\|\mathbf{f}_J\|^2 \leq \frac{\hat{c}_3}{L_J^2 \|\mathbf{w}_J\|^2} | \hat{\mathbf{f}}_J \right], \quad (21)$$

and

$$\begin{aligned} &\Pr \left[\|\mathbf{h}_l\|^2 \|\mathbf{w}_l\|^2 \leq (\hat{c}_l - A_l) | \hat{\mathbf{f}}_l, l = 0, 2 \right] \\ &= \Pr \left[\|\mathbf{f}_l\|^2 \leq \frac{(\hat{c}_l - A_l)}{L_l^2 \|\mathbf{w}_l\|^2} | \hat{\mathbf{f}}_l, l = 0, 2 \right]. \quad (22) \end{aligned}$$

According to Eqs. (7) and (8) and the distributions of $\hat{\mathbf{f}}_I$, $\hat{\mathbf{f}}_J$, \mathbf{e}_I , \mathbf{e}_J , we derive that $\|\mathbf{f}_l\|^2 \sim \mathcal{CN}(\|\hat{\mathbf{f}}_l\|^2, \|\mathbf{1}_K\|^2 \sigma_e^2)$, $l \in \{0, 2, 3\}$ follows a non-central chi-square distribution with two degrees of freedom [33]. Then, based on the cumulative distribution function (CDF) \mathcal{F} of the non-central chi-squared

distributed $\|\mathbf{f}_l\|^2, l \in \{0, 2, 3\}$, we respectively derive Eqs. (22) and (21) as

$$\begin{aligned} &\Pr \left[\|\mathbf{f}_l\|^2 \leq \frac{(\hat{c}_l - A_l)}{L_l^2 \|\mathbf{w}_l\|^2} | \hat{\mathbf{f}}_l, l = 0, 2 \right] = \frac{\epsilon_{\text{out}}}{2} \\ &= \mathcal{F}_{\|\mathbf{f}_l\|^2} \left(\frac{\hat{c}_l - A_l}{L_l^2 \|\mathbf{w}_l\|^2} \right), l = 0, 2 \quad (23) \\ &= 1 - Q_1 \left(\sqrt{\frac{2\|\hat{\mathbf{f}}_l\|^2}{\|\mathbf{1}_K\|^2 \sigma_e^2}}, \sqrt{\frac{2(\hat{c}_l - A_l)}{L_l^2 \|\mathbf{w}_l\|^2 \|\mathbf{1}_K\|^2 \sigma_e^2}} \right), l = 0, 2 \end{aligned}$$

and

$$\begin{aligned} &\Pr \left[\|\mathbf{f}_J\|^2 \leq \frac{\hat{c}_3}{L_J^2 \|\mathbf{w}_J\|^2} | \hat{\mathbf{f}}_J \right] = \frac{\epsilon_{\text{out}}}{2} \\ &= \mathcal{F}_{\|\mathbf{f}_J\|^2} \left(\frac{\hat{c}_3}{A_J^2 \|\mathbf{w}_J\|^2} \right), \quad (24) \\ &= 1 - Q_1 \left(\sqrt{\frac{2\|\hat{\mathbf{f}}_J\|^2}{\|\mathbf{1}_K\|^2 \sigma_e^2}}, \sqrt{\frac{2\hat{c}_3}{L_J^2 \|\mathbf{w}_J\|^2 \|\mathbf{1}_K\|^2 \sigma_e^2}} \right), \end{aligned}$$

where $Q_M(x, y) = \exp(-\frac{x^2+y^2}{2}) \sum_{k=1-M}^{\infty} \left(\frac{x}{y}\right)^k I_k(xy)$ is the Marcum Q-function. I_k is the first-kind k -th order modified Bessel function. Then, based on Eqs. (23) and (24), we have

$$\hat{c}_l = \mathcal{F}_{\|\mathbf{f}_l\|^2}^{-1} \left(\frac{\epsilon_{\text{out}}}{2} \right) L_l^2 \|\mathbf{w}_l\|^2 + A_l, l = 0, 2 \quad (25)$$

$$\hat{c}_3 = \mathcal{F}_{\|\mathbf{f}_J\|^2}^{-1} \left(\frac{\epsilon_{\text{out}}}{2} \right) L_J^2 \|\mathbf{w}_J\|^2, \quad (26)$$

where \mathcal{F}^{-1} is the inverse function of \mathcal{F} . As a result, we can derive the transformed expressions $\tilde{\gamma}_l$ of $\hat{\gamma}_l, l \in \{0, 2, 3\}$ as

$$\tilde{\gamma}_0 \triangleq \hat{\gamma}_0 = \frac{\hat{c}_0}{\hat{d}_0} = \frac{\mathcal{F}_{\|\mathbf{f}_l\|^2}^{-1} \left(\frac{\epsilon_{\text{out}}}{2} \right) L_I^2 \|\mathbf{w}_0\|^2 + |\mathbf{g}_{Rl}^H \Lambda \mathbf{G} \mathbf{w}_0|^2}{\sigma_I^2}, \quad (27)$$

$$\tilde{\gamma}_2 \triangleq \hat{\gamma}_2 = \frac{\hat{c}_2}{\hat{d}_2} = \frac{\mathcal{F}_{\|\mathbf{f}_l\|^2}^{-1} \left(\frac{\epsilon_{\text{out}}}{2} \right) L_I^2 \|\mathbf{w}_I\|^2 + |\mathbf{g}_{Rl}^H \Theta \mathbf{G} \mathbf{w}_I|^2}{\sigma_I^2}, \quad (28)$$

$$\tilde{\gamma}_3 \triangleq \hat{\gamma}_3 = \frac{\hat{c}_3}{\hat{d}_3} = \frac{\mathcal{F}_{\|\mathbf{f}_J\|^2}^{-1} \left(\frac{\epsilon_{\text{out}}}{2} \right) L_J^2 \|\mathbf{w}_J\|^2}{|\mathbf{g}_{Rl}^H \Theta \mathbf{G} \mathbf{w}_J|^2 + \sigma_J^2}. \quad (29)$$

Finally, substituting Eqs. (18) and (27)-(29) into the objective function in Eq. (12), the probabilistic mixed problem **P1** can be recast as the following problem

$$\begin{aligned} (\mathbf{P2}): \quad &\max_{\tau_1, \Theta, \mathbf{w}_I, \mathbf{w}_J} \tilde{O}_T = \sum_{l=0}^3 \rho_l \tilde{R}_l = \sum_{l=0}^3 \rho_l \log_2(1 + \tilde{\gamma}_l) \quad (30) \\ &\text{s.t.} \quad C_2 - C_7, \end{aligned}$$

where $\rho_0 = \frac{\tau_1}{\tau} (1 - \epsilon_{\text{out}})$ and $\rho_l = \frac{\tau - \tau_1}{\tau} P_l (1 - \epsilon_{\text{out}}), l \in \{1, 2, 3\}$, given $\Pr \left[\tilde{R}_l \leq R_l | \hat{\mathbf{f}}_l \right] = 1 - \epsilon_{\text{out}}, \forall l \in \{0, 1, 2, 3\}$.

IV. SOLUTION TO THE AVERAGE SYSTEMIC THROUGHPUT MAXIMIZATION PROBLEM

A. Problem Solution

This papers propose a fixed-point iterative (FPI) algorithm for solving the transformed **P2** by utilizing the QT method [34], [35] and typical convex optimization methods. The iterative optimizations of τ_1 , Θ , \mathbf{w}_I , \mathbf{w}_J are detailed as follows.

1) *Optimization of τ_1* : When Θ , \mathbf{w}_I , and \mathbf{w}_J are fixed, the optimization of τ_1 in **P2** can be expressed as

$$\begin{aligned} (\mathbf{P3} :) \max_{\tau_1} \quad & \tilde{O}_T = \sum_{l=0}^3 \rho_l(\tau_1) \tilde{R}_l \quad (31) \\ \text{s.t.} \quad & C2 : P_d(\tau_1) \geq \bar{P}_d \\ & C3 : P_f(\tau_1) \leq \bar{P}_f \\ & C7 : 0 < \tau_1 \leq \tau, \end{aligned}$$

where \tilde{R}_l is a constant term when Θ , \mathbf{w}_I , and \mathbf{w}_J are fixed.

Proposition 2: There exists a unique optimal τ_1^* to maximize \tilde{O}_T in problem **P3**.

Proof: According to Eq. (30), we get that

$$\rho_l(\tau_1) = \frac{\tau_1}{\tau} (1 - \epsilon_{\text{out}}), l = 0, \quad (32)$$

$$\rho_l(\tau_1) = \frac{\tau - \tau_1}{\tau} P_l(\tau_1) (1 - \epsilon_{\text{out}}), l \in \{1, 2, 3\}. \quad (33)$$

Based on the closed-form expressions of P_f , P_d , and $P_l(\tau_1), \forall l \in \{1, 2, 3\}$ in Section II, the proof of Proposition 2 can be implemented by deriving the first-order and second-order derivations of $\rho_l(\tau_1), \forall l \in \{0, 1, 2, 3\}$. Then, considering the feasible region for τ_1 in Eq. (31), the optimal τ_1^* can be numerically obtained by referring to the detailed derivations in Appendix of [24]. ■

Proposition 3: When τ_1 is fixed, the joint optimization of Θ , \mathbf{w}_I , \mathbf{w}_J in **P2** can be recast as a polynomial expression as follows

$$\begin{aligned} (\mathbf{P4} :) \max_{\Theta, \mathbf{w}_I, \mathbf{w}_J, \mathbf{u}, \mathbf{v}, \mathbf{y}} \quad & \tilde{O}_T^Q = \sum_{m=1}^4 \rho_m \log_2(1 + v_m) - \rho_m v_m \quad (34) \\ & + \sum_{m=1}^4 2\sqrt{\rho_m(1 + v_m)} \xi_m \Re_m \\ & - |u_1|^2 \sigma_1^2 - |u_4|^2 \sigma_4^2 \\ & - \sum_{m=2}^3 \|\mathbf{y}_m\|^2 \sigma_m^2 \\ \text{s.t.} \quad & C4 : \|\mathbf{w}_I\|^2 \leq p_{I\max} \\ & C5 : \|\mathbf{w}_J\|^2 \leq p_{J\max} \\ & C6 : |\mathbf{g}_{RJ}^H \Theta \mathbf{G} \mathbf{w}_I|^2 \leq \bar{\epsilon}_J, \end{aligned}$$

where $\mathbf{u} = [u_1, u_4]$, u_1 and u_4 are two auxiliary complex variables. $\mathbf{y} = [\mathbf{y}_2^H, \mathbf{y}_3^H]^H$ in which $\mathbf{y}_2 \in \mathbb{C}^{K \times 1}$ and $\mathbf{y}_3 \in \mathbb{C}^{K \times 1}$ are two complex vectors. $\mathbf{v} = [v_1, v_2, v_3, v_4]$ is an auxiliary real vector. ρ_1, ρ_2, ρ_3 are given in Eq. (30) and $\rho_4 = \rho_2$. $\xi_1 = \epsilon_{\text{out}}$, $\xi_2 = \mathcal{F}_{\|\hat{\mathbf{f}}_I\|^2}^{-1}(\frac{\epsilon_{\text{out}}}{2}) L_I^2$, $\xi_3 = \mathcal{F}_{\|\hat{\mathbf{f}}_J\|^2}^{-1}(\frac{\epsilon_{\text{out}}}{2}) L_J^2$, and $\xi_4 = 1$. $\sigma_1^2 = 2L_I^2(\|\hat{\mathbf{f}}_I\|^2 + \|\mathbf{1}_K\|^2 \sigma_e^2) \|\mathbf{w}_J\|^2 + \epsilon_{\text{out}} \sigma_I^2$, $\sigma_4^2 = \sigma_2^2 = \sigma_I^2$, $\sigma_3^2 = |\mathbf{g}_{RJ}^H \Theta \mathbf{G} \mathbf{w}_I|^2 +$

$$\sigma_{J.}^2 \Re_m = \begin{cases} \text{Re}\{u_1^H \mathbf{g}_{RI}^H \Theta \mathbf{G} \mathbf{w}_I\}, & m = 1 \\ \text{Re}\{\mathbf{y}_2^H \mathbf{w}_I\}, & m = 2 \\ \text{Re}\{\mathbf{y}_3^H \mathbf{w}_J\}, & m = 3 \\ \text{Re}\{u_4^H \mathbf{g}_{RI}^H \Theta \mathbf{G} \mathbf{w}_I\}, & m = 4 \end{cases}$$

Proof: The proof is mainly based on the QT method and Lagrangian dual transform method in [34], [35]. Please refer to Appendix B. ■

Based on the Proposition 3, the iterative optimizations of \mathbf{v} , \mathbf{u} , \mathbf{y} , \mathbf{w}_J , \mathbf{w}_I , and Θ are detailed as follows.

2) *Optimize \mathbf{v}* : Given \mathbf{u} , \mathbf{y} , \mathbf{w}_J , \mathbf{w}_I , and Θ , $-|u_1|^2 \sigma_{D,1}^2 - |u_4|^2 \sigma_{D,4}^2 - \sum_{m=2}^3 \|\mathbf{y}_m\|^2 \sigma_{D,m}^2$ is a constant term in **P4**. Therefore, the optimization of \mathbf{v} can be recast as

$$\begin{aligned} \max_{\mathbf{v}} \quad & \tilde{O}_T^Q = \sum_{m=1}^4 \rho_m \log_2(1 + v_m) - \rho_m v_m \quad (35) \\ & + \sum_{m=1}^4 2\sqrt{\rho_m(1 + v_m)} \xi_m \Re_m. \end{aligned}$$

According to the concavities of $\log_2(\cdot)$ function and square-root $\sqrt{\cdot}$ function, it's obvious that \tilde{O}_T^Q is concave over \mathbf{v} . Therefore, the optimal \mathbf{v}^* can be obtained by solving $\frac{\partial \tilde{O}_T^Q(v_m)}{\partial v_m} = 0$ as

$$v_m^* = \frac{\xi_m \Re_m^2 + \Re_m \sqrt{\xi_m^2 \Re_m^2 + 4\xi_m \rho_m}}{2\rho_m}, \forall m. \quad (36)$$

3) *Optimize \mathbf{u} and \mathbf{y}* : Given \mathbf{v} , \mathbf{w}_J , \mathbf{w}_I , Θ , $\sum_{m=1}^4 \rho_m \log_2(1 + v_m) - \rho_m v_m + 2\sqrt{\rho_m(1 + v_m)} \xi_m \Re_m$ is a constant term in problem **P4**. Therefore, the optimizations of \mathbf{u} and \mathbf{y} can be recast as

$$\begin{aligned} \max_{\mathbf{u}, \mathbf{y}} \quad & \tilde{O}_T^Q = -|u_1|^2 \sigma_1^2 - |u_4|^2 \sigma_4^2 - \sum_{m=2}^3 \|\mathbf{y}_m\|^2 \sigma_m^2 \quad (37) \\ & + \sum_{m=1}^4 2\sqrt{\rho_m(1 + v_m)} \xi_m \Re_m. \end{aligned}$$

Based on the concavity of $-x^2$ function and the linearity of \Re_m over \mathbf{u}, \mathbf{y} , we get that \tilde{O}_T^Q is concave over \mathbf{u} and \mathbf{y} , respectively. Therefore, the optimal \mathbf{u}^* and \mathbf{y}^* can be obtained by solving $\frac{\partial \tilde{O}_T^Q(u_m)}{\partial u_m} = 0, m = 1, 4$, and $\frac{\partial \tilde{O}_T^Q(\mathbf{y}_m)}{\partial \mathbf{y}_m} = 0, m = 2, 3$, respectively. Consequently, we obtain

$$u_m^* = \frac{\zeta_m \sqrt{\rho_m(1 + v_m)} \xi_m}{\sigma_m^2}, m = 1, 4 \quad (38)$$

$$y_m^* = \frac{\zeta_m \sqrt{\rho_m(1 + v_m)} \xi_m}{\sigma_m^2}, m = 2, 3 \quad (39)$$

where $\zeta_1 = \mathbf{g}_{RI}^H \Theta \mathbf{G} \mathbf{w}_I$, $\zeta_2 = \mathbf{w}_I$, $\zeta_3 = \mathbf{w}_J$.

4) *Optimize \mathbf{w}_J* : Given \mathbf{v} , \mathbf{u} , \mathbf{y} , \mathbf{w}_I and Θ , $\sum_{m=1}^4 \rho_m \log_2(1 + v_m) - \rho_m v_m - |u_1|^2 \epsilon_{\text{out}} \sigma_I^2 - |u_4|^2 \sigma_4^2 - \sum_{m=2}^3 \|\mathbf{y}_m\|^2 \sigma_m^2 + \sum_{m \in \{1, 2, 4\}} 2\sqrt{\rho_m(1 + v_m)} \xi_m \Re_m$ is a constant term in **P4**. Therefore, the optimization of \mathbf{w}_J can be recast as

$$\begin{aligned} \max_{\mathbf{w}_J} \quad & \tilde{O}_T^Q = -|u_1|^2 c_J \|\mathbf{w}_J\|^2 \quad (40) \\ & + 2\sqrt{\rho_3(1 + v_3)} \xi_3 \text{Re}\{\mathbf{y}_3^H \mathbf{w}_J\} \\ \text{s.t.} \quad & \|\mathbf{w}_J\|^2 \leq p_{J\max}, \end{aligned}$$

where $c_J = 2L_J^2(\|\hat{\mathbf{f}}_I\|^2 + \|\mathbf{1}_K\|^2 \sigma_e^2)$. The \tilde{O}_T^Q in Eq. (40) is convex about \mathbf{w}_J with the convex constraint. Therefore, utilizing the Lagrange multiplier method [7], the optimal \mathbf{w}_J^* can be obtained as

$$\mathbf{w}_J^* = \sqrt{\rho_3(1 + v_3)} \xi_3 (|u_1|^2 c_J + \eta_J \mathbf{I}_K)^{-1} \mathbf{y}_3, \quad (41)$$

where η_J is the dual variable introduced for the maximum power constraint of \mathbf{w}_J . The optimal η_J^* can be obtained as $\eta_J^* = \min\{\eta_J \geq 0 : \|\mathbf{w}_J(\eta_J)\|^2 \leq p_{J\max}\}$ through the bisection search method [34].

5) *Optimize \mathbf{w}_I* : Given \mathbf{v} , \mathbf{u} , \mathbf{y} , \mathbf{w}_J and Θ , $\sum_{m=1}^4 \rho_m \log_2(1 + v_m) - \rho_m v_m + 2\sqrt{\rho_3(1 + v_3)}\xi_3\mathfrak{R}_3 - |u_1|^2\sigma_1^2 - |u_4|^2\sigma_4^2 - \sum_{m=1}^2 \|\mathbf{y}_m\|^2\sigma_m^2$ is a constant term in problem P4. Therefore, the optimization of \mathbf{w}_I is recast as

$$\max_{\mathbf{w}_I} \tilde{O}_T^Q = -\|\mathbf{y}_3\|^2 \mathbf{w}_I^H \mathbf{\Gamma} \mathbf{\Gamma}^H \mathbf{w}_I - \|\mathbf{y}_3\|^2 \sigma_J^2 + 2\text{Re}\{\zeta^H \mathbf{w}_I\} \quad (42)$$

$$\text{s.t.} \quad \|\mathbf{w}_I\|^2 \leq p_{I\max} \\ |\mathbf{g}_{RJ}^H \Theta \mathbf{G} \mathbf{w}_I|^2 \leq \bar{\epsilon}_J,$$

where $\mathbf{\Gamma}^H = \mathbf{g}_{RJ}^H \Theta \mathbf{G}$, $\zeta^H = \sum_{m \in \{1,2,4\}} \sqrt{\rho_m(1+v_m)} \xi_m \lambda_m^H$, $\lambda_1^H = u_1^H \mathbf{g}_{R1}^H \Theta \mathbf{G}$, $\lambda_2^H = \mathbf{y}_2^H$, $\lambda_4^H = u_4^H \mathbf{g}_{R4}^H \Theta \mathbf{G}$.

The problem in (42) is a quadratically constrained quadratic problem (QCQP) [7] about \mathbf{w}_I . Therefore, utilizing Lagrange multiplier method, the optimal \mathbf{w}_I^* can be obtained as

$$\mathbf{w}_I^* = (\|\mathbf{y}_3\|^2 \mathbf{\Gamma} \mathbf{\Gamma}^H + \eta_I \mathbf{I}_K)^{-1} \zeta, \quad (43)$$

where η_I is the dual variable introduced for the constraints of \mathbf{w}_I . Similarly, the optimal η_I^* can be obtained as $\eta_I^* = \min\{\eta_I \geq 0 : \|\mathbf{w}_I(\eta_I)\|^2 \leq p_{I\max}\} \cap \{\mathbf{w}_I^H(\eta_I) \mathbf{\Gamma} \mathbf{\Gamma}^H \mathbf{w}_I(\eta_I) \leq \bar{\epsilon}_J\}$ by utilizing the bisection search method.

6) *Optimize Θ* : Given \mathbf{v} , \mathbf{u} , \mathbf{y} , \mathbf{w}_J and \mathbf{w}_I , $\sum_{m=1}^4 \rho_m \log_2(1 + v_m) - \rho_m v_m - |u_1|^2 \sigma_1^2 - |u_4|^2 \sigma_4^2 - \|\mathbf{y}_2\|^2 \sigma_2^2 + \sum_{m=2}^3 2\sqrt{\rho_m(1+v_m)}\xi_m\mathfrak{R}_m$ is a constant term in problem P4. Therefore, the optimization of $\Theta = \text{diag}(\psi = [e^{j\theta_1}, \dots, e^{j\theta_{N_R}}]^T)$ can be recast as⁵

$$\max_{\Theta} \tilde{O}_T^Q = -\|\mathbf{y}_3\|^2 \psi^H \mathbf{\Pi} \psi - \|\mathbf{y}_3\|^2 \sigma_J^2 + 2\text{Re}\{\psi^H \delta\} \quad (44) \\ \text{s.t.} \quad \psi^H \mathbf{\Pi} \psi \leq \bar{\epsilon}_J,$$

where $\mathbf{\Pi} = (\text{diag}(\mathbf{G} \mathbf{w}_I))^H \mathbf{g}_{RJ} \mathbf{g}_{RJ}^H (\text{diag}(\mathbf{G} \mathbf{w}_I))$, $\delta = \sum_{m \in \{1,4\}} \sqrt{\rho_m(1+v_m)} \xi_m \text{diag}(u_m^H \mathbf{g}_{Rm}^H) \mathbf{G} \mathbf{w}_I$.

The problem in (44) is also a QCQP over Θ . Therefore, based on the Lagrange multiplier method, the optimal ψ^* can be obtained as

$$\psi^* = \|\mathbf{y}_3\|^2 (\mathbf{\Pi} + \eta_{\Theta} \mathbf{I}_{N_R})^{-1} \delta, \quad (45)$$

where η_{Θ} is the dual variable introduced for the constraint of ψ . Similarly, utilizing the bisection search method, the optimal η_{Θ}^* can be obtained as $\eta_{\Theta}^* = \min\{\eta_{\Theta} \geq 0 : \psi^H(\eta_{\Theta}) \mathbf{\Pi} \psi(\eta_{\Theta}) \leq \bar{\epsilon}_J/p_I\}$.

Ultimately, the proposed FPI algorithm for solving the AST maximization problem P2 is summarized in Algorithm 1.

⁵Note that the practical discrete phase shift design involves additional constraint $\theta_{n_R} \in \mathcal{F}$, $\forall n_R \in \{1, \dots, N_R\}$, where $\mathcal{F} = \{0, 2\pi/L, \dots, 2\pi(L-1)/L\}$ is the set of discrete phase shift values. $L = 2b$ is the number of phase shift levels, and b represents the phase resolution in bits. Combining with the semi-definite relaxation (SDR) method, we can heuristically obtain the sub-optimal discrete phase shift ψ by directly mapping each phase shift in ψ^* to its nearest discrete value in \mathcal{F} . The larger b comes to the larger number of phase shift levels L , leading to ψ being closer to the optimal continuous phase shift ψ^* . Otherwise, a smaller b degrades the optimality of RIS phase shift design, which inevitably degrades the RIS-assisted communication performance obtained at the PC period and further degrades the AST, as expressed in Eqs. (10) and (11). In a word, the optimal continuous RIS phase shift obtained in this research gives an examination of the upper-bound systemic communication performance of the proposed R-SACE mechanism.

Algorithm 1 FPI Algorithm for Solving AOSC Maximization Problem

INITIALIZE: $\tau_1(0)$, $\Theta(0)$, $\mathbf{w}_I(0)$, $\mathbf{w}_J(0)$, \mathbf{u} , \mathbf{y} , and \mathbf{v} , $t \leftarrow 1$

Repeat

Part 1:

Update $\tau_1^*(t)$ by numerically solving the convex problem P3, given $\Theta(t-1)$, $\mathbf{w}_I(t-1)$, and $\mathbf{w}_J(t-1)$,

Part 2:

Update $\mathbf{v}^*(t)$ by Eq. (36), given $\tau_1^*(t)$, $\mathbf{u}(t-1)$, $\mathbf{y}(t-1)$, $\mathbf{w}_I(t-1)$, $\mathbf{w}_J(t-1)$, and $\Theta(t-1)$,

Update $\mathbf{u}^*(t)$ and $\mathbf{y}^*(t)$ by Eqs. (38) and (39) respectively, given $\tau_1^*(t)$, $\mathbf{v}^*(t)$, $\mathbf{w}_I(t-1)$, $\mathbf{w}_J(t-1)$, and $\Theta(t-1)$,

Update $\mathbf{w}_J^*(t)$ by Eq. (41), given $\tau_1^*(t)$, $\mathbf{v}^*(t)$, $\mathbf{u}^*(t)$, $\mathbf{y}^*(t)$, $\mathbf{w}_I(t-1)$, and $\Theta(t-1)$,

Update $\mathbf{w}_I^*(t)$ by Eq. (43), given $\tau_1^*(t)$, $\mathbf{v}^*(t)$, $\mathbf{u}^*(t)$, $\mathbf{y}^*(t)$, $\mathbf{w}_J^*(t)$, and $\Theta(t-1)$,

Update $\Theta^*(t)$ by Eq. (45), given $\tau_1^*(t)$, $\mathbf{v}^*(t)$, $\mathbf{u}^*(t)$, $\mathbf{y}^*(t)$, $\mathbf{w}_J^*(t)$, and $\mathbf{w}_I^*(t)$,

Calculate $\tilde{O}_T(\tau_1^*(t))$, $\Theta^*(t)$, $\mathbf{w}_I^*(t)$, $\mathbf{w}_J^*(t)$, $t = t + 1$,

Until

$\tilde{O}_T(\tau_1^*(t))$, $\Theta^*(t)$, $\mathbf{w}_I^*(t)$, $\mathbf{w}_J^*(t) - \tilde{O}_T(\tau_1^*(t-1))$, $\Theta^*(t-1)$, $\mathbf{w}_I^*(t-1)$, $\mathbf{w}_J^*(t-1) \leq \Delta$, Δ is the convergence threshold.

RETURN: The optimal solution τ_1^* , Θ^* , \mathbf{w}_I^* , \mathbf{w}_J^* of P2.

B. Convergence and Complexity Analysis

We first analyze the convergence of the proposed FPI algorithm. As presented in Algorithm 1, there are Part 1 and Part 2 to solve the optimization of τ_1 and the joint optimization of Θ , \mathbf{w}_I , \mathbf{w}_J , respectively. As presented in Proposition 2, the optimal $\tau_1^*(t)$ can be numerically obtained by calculating the first- and second-order derivatives of $\rho_l(\tau_1)$, $\forall l$. Therefore, we only need to analyze the convergence of Part 2 in Algorithm 1. Given $\tau_1(t)$, the closed-form optimal $\mathbf{w}_J^*(t)$, $\mathbf{w}_I^*(t)$, and $\Theta^*(t)$ can be obtained through the fixed-point QT method, according to Eqs. (41), (43), and (45), respectively. The convergence of the fixed-point QT method to iteratively optimize variables has been established in detail in Appendix A of [35]. Therefore, the part 2 in Algorithm 1 is convergent. Finally, the \tilde{O}_T in Eq. (30) increases with each optimal iterations of $\tau_1^*(t)$, $\Theta^*(t)$, $\mathbf{w}_I^*(t)$, and $\mathbf{w}_J^*(t)$ in Algorithm 1. Therefore, the overall convergence of the proposed FPI algorithm is guaranteed.

Next, we analyze the complexity of the proposed FPI algorithm. According to Proposition 2, the optimal τ_1^* is obtained by numerically calculating the first- and second-order derivatives of \tilde{O}_T over τ_1 . Therefore, the complexity of optimizing τ_1 in Part 1 in Algorithm 1 is $\mathcal{O}(1)$, regardless of the number of RIS elements and communication users. This demonstrates the computational efficiency of FPI algorithm in optimizing the temporal resource allocation in ISAC systems. Then, according to Proposition 3, the fixed-point QT method recasts the joint optimization of Θ , \mathbf{w}_I , and \mathbf{w}_J as a series of convex problems in Eqs. (35)-(45), where the closed-form optimal solutions are obtained through the bisection search method. Let I_{Θ} , I_{w_1} , and I_{w_2} denote the maximal iterations of obtaining optimal Θ^* , \mathbf{w}_I^* , and \mathbf{w}_J^* through the bisection search method. The complexity

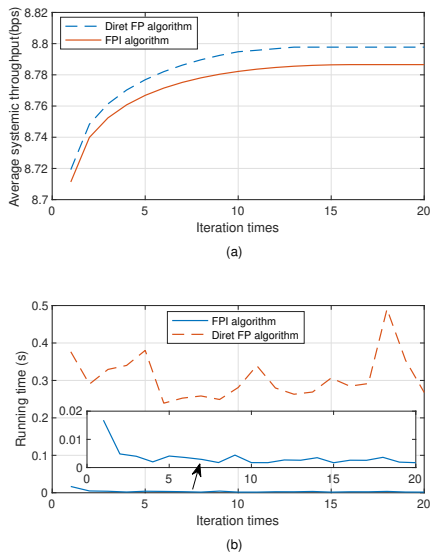


Fig. 3. A comparison of the convergence iterations and running time of different algorithms. (a) Convergence iteration. (b) Running time.

of jointly optimizing $\Theta^*(t)$, $\mathbf{w}_J^*(t)$, and $\mathbf{w}_I^*(t)$ in Part 2 in Algorithm 1 can be obtained as $\mathcal{O}(\max\{I_\Theta, I_{w1}, I_{w2}\})$. It's worth mentioning that with a larger N_R , the optimal Θ^* can also be obtained through the closed-form solution in Eq. (45). The iteration number of the bisection search to find the dual variable η_θ remains unaffected. Therefore, the complexity of optimizing Θ^* does not increase with the number of RIS elements. Similarly, with larger number of TC J or CU I , the complexities of optimizing $\mathbf{w}_J^*(t)$ for each TC J and optimizing $\mathbf{w}_I^*(t)$ for each CU I also remain unchanged. Then, let I_O denote the maximal iterations of the repeat operation in Algorithm 1. The complexity order of Algorithm 1 can be finally obtained as $\mathcal{O}(I_O * \max\{1, \max\{I_\Theta, I_{w1}, I_{w2}\}\}) = \mathcal{O}(I_O * \max\{I_\Theta, I_{w1}, I_{w2}\})$. Note that, although I_O increases with more TC J and CU I , it is still a finite number. Therefore, the complexity of solving AST maximization problem through the FPI algorithm is polynomial regardless of larger RIS configurations or more communication users.

We further analyze the convergence and running time of the adopted FPI algorithm compared with the direct fractional programming (FP) algorithm [34], [35] in Fig. 3. In the direct FP algorithm, each iteration is performed by numerically solving a convex optimization problem, rather than in closed form as in the FPI algorithm. As shown in this figure, the adopted FPI algorithm takes more iterations to converge, but its running time per iteration is the lowest, thanks to the closed-form updates in each iteration. In summary, the adopted FPI algorithm is the fastest, resulting in greater practicality.

V. SIMULATION RESULTS

This section evaluates the effectiveness of the proposed FPI algorithm and the R-SACE mechanism in comparison to baseline algorithms and mechanisms. The specific simulation parameters are set as follows. The location coordinates for BS, CU I , TC J , and RIS are set as $(-20, 20)$, $(20, 0)$, $(0, 10)$, and $(-5, 15)$, respectively. Referring to [7], we set the large-scale

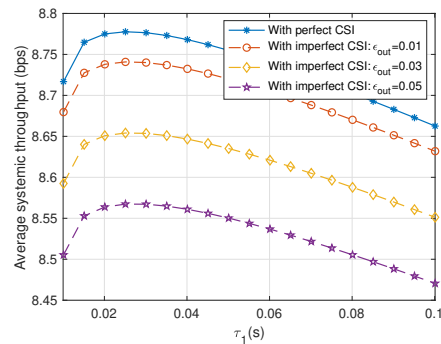


Fig. 4. The AST obtained with perfect and imperfect CSIs changing with τ_1 .

path loss in this paper as $A_0(\frac{d_X}{d_0})^{-\alpha}$, where $A_0 = -30\text{dB}$ denotes the path loss at reference distance $d_0 = 1\text{m}$. d_X , $X \in \{BR, RI, RJ, I, J\}$, denotes the distance of BS-RIS, RIS-CU I , RIS-TC J , BS-CU I , and BS-TC J . α denotes the path-loss exponent. In particular, $\alpha_{BR} = 2.5$, $\alpha_{RI} = 2.5$, $\alpha_{RJ} = 2.5$, $\alpha_J = 3$, and $\alpha_I = 3.5$ for \mathbf{g}_{RI} , \mathbf{g}_{RJ} , $\hat{\mathbf{h}}_J$, and $\hat{\mathbf{h}}_I$, respectively. Generally, $\mathbf{G} = \beta_G(\sqrt{g}\mathbf{G}^{\text{LoS}} + \sqrt{1-g}\mathbf{G}^{\text{NLoS}})$ follows Rician distribution [9], [11], where $\beta_G = \sqrt{\frac{A_0}{d_{BR}^{\alpha_{BR}}}}$ is distance dependent path loss, $g = 0.8$ is Rician coefficient. $\mathbf{G}^{\text{LoS}} = \mathbf{a}_{N_R}(\theta_{RB})\mathbf{a}_K^H(\theta_{BR})$ is the deterministic LoS component [9], [11]. \mathbf{a}_{N_R} and \mathbf{a}_K represent the steering vector and θ_{RB} and θ_{BR} represent the DoA and DoD. Each element in the non-LoS component \mathbf{G}^{NLoS} follows $\mathcal{CN}(0, 1)$. Referring to [13], the duration of the entire timeline is $\tau = 1\text{s}$. Additionally, $f_s = 10\text{MHz}$, $K = 4$, $N_R = 16$, $\sigma^2 = \sigma_0^2 = \sigma_I^2 = \sigma_J^2 = -110\text{dBm}$, $P_{J_1} = P_{J_0} = 0.5$, and $\sigma_T^2 = 1$ as referred to [11].

A. Performance Evaluation

Fig. 4 shows the difference between AST obtained with perfect CSI and imperfect CSI. This figure demonstrates that the AST obtained with imperfect CSI is lower than the upper-bound AST obtained with perfect CSI. Whereas, the gap in AST decreases with the probability threshold ϵ_{out} . This is because lower ϵ_{out} helps achieve more desirable systemic communication performance by limiting the error probability of channel estimation to a lower level. Additionally, this figure shows that for every curve, there is an optimal τ_1^* to maximize the AST. This is because increasing τ_1 helps obtain more reliable sensing results, which facilitate communication during the PC period. However, increasing τ_1 also reduces the time $\tau - \tau_1$ for communication in the PC period. Therefore, there exists an optimal time allocation τ_1^* between ISAC and PC periods for achieving satisfied sensing performance and eventually contributing to the maximal communication performance AST. This simulation result further verifies the correctness of the theoretical analysis in Proposition 2.

Fig. 5 illustrates the sensing performance obtained at the ISAC period changing with the noise power σ^2 . The false alarm probability \bar{P}_f obtained at the BS is fixed as 0.1 in this simulation and thus remains unchangeable with the noise power. In this simulation, we introduce two additional sensing performance metrics: the error probability $P_E = P_{J_1}(1 - P_d) +$

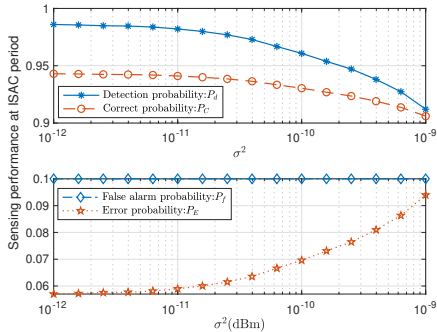


Fig. 5. The sensing performance obtained at ISAC period changing with σ^2 .

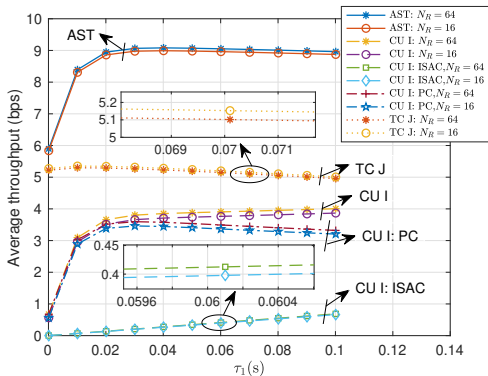


Fig. 6. The average throughput changing with τ_1 and N_R .

$(1 - P_{J1})P_f$ and the correct probability $P_C = 1 - P_E$, for comprehensively evaluating the systemic sensing performance. As illustrated in this figure, with a fixed false alarm probability, the detection probability P_d decreases with the noise power σ^2 . Furthermore, the degraded detection probability leads to a lower correct probability P_C and inevitably an increased error probability as noise power rises. Fortunately, the correct probability remains greater than 0.9, and the error probability does not exceed 0.1, even when the noise power is as large as 10^{-9} dBm. This simulation result demonstrates the robustness of the proposed R-SACE mechanism in maintaining satisfactory sensing performance.

Fig. 6 presents the contributions of AST from CU I and TC J changing with τ_1 and the number of RIS elements N_R . It is clear that the average throughput of CU I during the ISAC period increases with τ_1 , owing to the longer communication time. During the PC period, the average throughput of CU I initially increases and then decreases with τ_1 . This phenomenon can be explained as follows. First, the sensing performance, i.e., the correct probability about TC J , is enhanced with the increased sensing time τ_1 , leading to a higher average throughput for CU I during the PC period. Whereas as τ_1 increases, the communication time $\tau - \tau_1$ during the PC period decreases, resulting in a lower average throughput of CU I during this period. The overall average throughput of CU I throughout the entire timeline increases with τ_1 because the communication performance contribution from the ISAC period is greater than that from

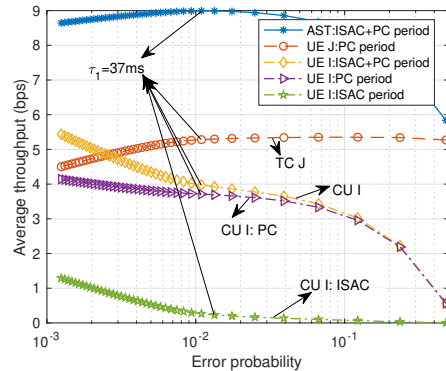


Fig. 7. The average throughput vs. error probability.

the PC period. Regarding TC J , its average throughput during the PC period first increases and then decreases with τ_1 . Specifically, the improved average throughput results from enhanced sensing accuracy, which increases with τ_1 and allows for better transmission coordination between CU I and TC J . Whereas, the lower average throughput is a result of the decreased communication time. Finally, the AST first increases and then decreases with τ_1 . This phenomenon indicates that TC J has a greater contribution to AST than CU I . Moreover, this result demonstrates that an optimal balance between S&C in time resource allocation exists and must be achieved to maximize the AST of the proposed R-SACE mechanism.

Fig. 6 further shows that the average throughput of CU I increases with the number of RIS elements during the ISAC period, PC period, and the entire period. This result is because the larger N_R enhances the received signal strength from the BS-RIS-CU I link, thereby contributing to a higher communication SINR for CU I . As for the TC J , its average throughput decreases with N_R . This is due to the increased number of RIS elements resulting in severe interference from the BS-RIS-CU I link. Finally, the AST increases with N_R , since the RIS-assisted increment in the average throughput of CU I is greater than the decrement in the average throughput of TC J . This result demonstrates the effectiveness of utilizing RIS in improving systemic communication performance of the proposed R-SACE mechanism by coordinating transmission and suppressing mutual interference.

Fig. 7 presents the trade-off between S&C performances affected by time resource allocation in the proposed R-SACE mechanism. The average throughputs and the error probability are presented in this figure. In this figure, the average throughput of CU I during the ISAC period increases as the error probability P_E decreases. This is due to the longer duration τ_1 leading to a lower P_E and a higher average throughput of CU I during the ISAC period. During the PC period, the average throughput of CU I increases as the error probability P_E decreases. This phenomenon can be explained as follows. As τ_1 increases, the improvement in communication performance of CU I , which benefits from the continuously decreasing P_E , offsets the decrease in average throughput of CU I caused by the reduced duration of the PC period as shown in Fig. 6. Therefore, the overall average

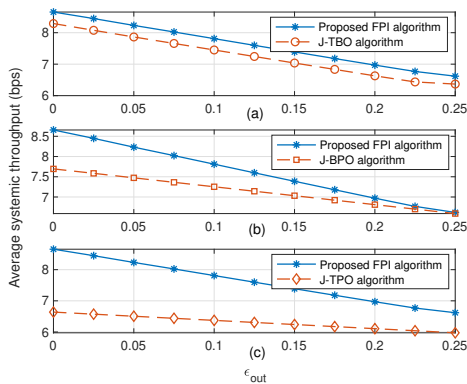


Fig. 8. The AST v.s. ϵ_{out} obtained with different algorithms.

throughput of CU I during the entire timeline increases as the error probability decreases. For TC J , the average throughput first increases and then decreases as P_E decreases. This result demonstrates that there exists an optimal S&C time allocation between ISAC and PC periods, which maximizes sensing-assisted communication performance for TC J . Finally, we can observe that a maximal AST exists when $\tau_1 = 37$ ms, as the error probability P_E varies. This result shows that an optimal S&C time allocation exists for achieving the maximal systemic communication performance. More importantly, this result demonstrates that the proposed R-SACE mechanism optimally balances the resource competition and functional assistance between S&C, leading to maximal systemic communication performance. Last but not least, after $\tau_1 = 37$ ms, the reduction in AST becomes much more serious, even when the increase in error probability P_E is minimal. This highlights the need for improving detection accuracy using effective methods, such as the adaptive threshold method [39].

B. Comparisons of optimization algorithms

In this subsection, we evaluate the effectiveness of the proposed FPI algorithm in obtaining higher AST by jointly optimizing time allocation, transmission beamforming, and phase shift of RIS. Three baseline algorithms are presented for comparison: the joint beamforming and phase shift optimization (J-BPO) algorithm [36], the joint time allocation and phase shift optimization (J-TPO) algorithm [24], and the joint time allocation and beamforming optimization (J-TBO) algorithm. In the J-BPO, J-TPO, and J-TBO algorithms, the time allocation τ_1 , the beamforming \mathbf{w}_I and \mathbf{w}_J , and the phase shift Θ are randomly designed, respectively.

Fig. 8(a) shows the superiority of the proposed FPI algorithm in achieving higher AST than the J-TBO algorithm. The reason is that the phase shift Θ of RIS is randomly designed in the J-TBO algorithm. While in the proposed FPI algorithm, Θ is jointly optimized with time allocation τ_1 and transmission beamforming, which thus helps further improve the systemic communication performance of the R-SACE mechanism. Fig. 8(b) shows that the proposed FPI algorithm achieves higher AST than the J-BPO algorithm. This advantage is attributed to that optimizing the time allocation τ_1 between ISAC and

PC periods in the FPI algorithm contributes to better coordination of S&C performances. In other words, compared to the randomly designed ISAC time protocol in the J-BPO algorithm, optimizing τ_1 in the FPI algorithm guarantees the sensing performance that further helps improve the systemic communication performance of the R-SACE mechanism.

Fig. 8(c) shows that the proposed FPI algorithm achieves higher AST than the J-TPO algorithm by further optimizing the transmission beamforming \mathbf{w}_I and \mathbf{w}_J . More specifically, in contrast to the randomly designed beamforming in J-TPO algorithm, the joint optimization of \mathbf{w}_I and \mathbf{w}_J in the FPI algorithm helps coordinate the communication performances of two UEs and hence contributes to the improvement of the systemic communication performance. Moreover, as we can see in Fig. 8, the AST obtained through differently algorithms decreases with ϵ_{out} . This result is because that the lower ϵ_{out} means the lower probability that the data rates obtained with imperfect CSI exceed the achievable data rates obtained with perfect CSI. In other words, the lower ϵ_{out} restricts the outage probability of the data rate obtained with imperfect CSI, which thus contributes to a higher AST. This result can be further verified by the theoretical analysis in Eq. (30).

C. Comparisons of communication enhancement mechanisms

In this subsection, we evaluate the effectiveness of the proposed R-SACE mechanism by comparing with two baseline mechanisms, i.e., the RIS-assisted communication enhancement (R-ACE) mechanism [37] and the sensing-assisted communication enhancement (S-ACE) mechanism [38]. The main differences among these mechanisms lie in that in the ISAC period, the proposed R-SACE mechanism performs both sensing and communication, while the R-ACE mechanism only performs communication and the S-ACE mechanism only performs sensing. Table I summarizes different mechanisms. Note that the communication performances of R-ACE and S-ACE mechanism are evaluated with imperfect CSI also. Then, we first detail the communication performances of the R-ACE and the S-ACE mechanisms, respectively.

In the R-ACE mechanism, the BS does not sense but communicates with CU I during the ISAC period, where the average data rate of CU I is the same as in the R-SACE mechanism. Without sensing, the BS assumes the probability of TC J being present as P_{AJ} during the PC period. When the BS assumes that TC J is present, it communicates with CU I via the BS-RIS-CU I link while simultaneously communicating with TC J via the BS-TC J link. Otherwise, when the BS assumes TC J is not present, it communicates with CU I via both the BS-RIS-CU I link and the BS-CU I link. As a result, the average data rate of the present TC J in the PC period is given by $P_J^R \log_2(1 + \hat{\gamma}_J^{(1)})$, where $P_J^R = P_{AJ}P_{J_1}$ and $\hat{\gamma}_J^{(1)}$ is given in Eq. (10). The average data rate of CU I in the PC period is given by $P_{AJ} \log_2(1 + \hat{\gamma}_I^{R(1)}) + (1 - P_{AJ}) \log_2(1 + \hat{\gamma}_I^{R(0)})$, where $\hat{\gamma}_I^{R(1)} = \hat{\gamma}_{I(2)}^{(1)}$ and $\hat{\gamma}_I^{R(0)} = \hat{\gamma}_{I(2)}^{(0)}$, as shown in Eq. (10). The constraints in the R-ACE mechanism are the same as those in the R-SACE mechanism.

In the S-ACE mechanism, the BS performs sensing during the ISAC period and then uses the sensing results to aid

TABLE II
COMPARISONS OF DIFFERENT COMMUNICATION ENHANCE MECHANISMS WITH IMPERFECT CSI

Mechanisms	ISAC Period		PC Period	
	Sensing	Communication	Average data rate of CU I	Average data rate of TC J
R-SACE	✓	$\log_2(1 + \hat{\gamma}_{I(1)})$	$P_{I(2)}^{(1)} \log_2(1 + \hat{\gamma}_{I(2)}^{(1)}) + P_{I(2)}^{(0)} \log_2(1 + \hat{\gamma}_{I(2)}^{(0)})$	$P_J^{(1)} \log_2(1 + \hat{\gamma}_J^{(1)})$
R-ACE	✗	$\log_2(1 + \hat{\gamma}_{I(1)})$	$P_{AJ} \log_2(1 + \hat{\gamma}_I^{R(1)}) + (1 - P_{AJ}) \log_2(1 + \hat{\gamma}_I^{R(0)})$	$P_J^R \log_2(1 + \hat{\gamma}_J^{(1)})$
S-ACE	✓	✗	$P_{I(2)}^{(1)} \log_2(1 + \hat{\gamma}_I^{S(1)}) + P_{I(2)}^{(0)} \log_2(1 + \hat{\gamma}_I^{S(0)})$	$P_J^{(1)} \log_2(1 + \hat{\gamma}_J^{S(1)})$

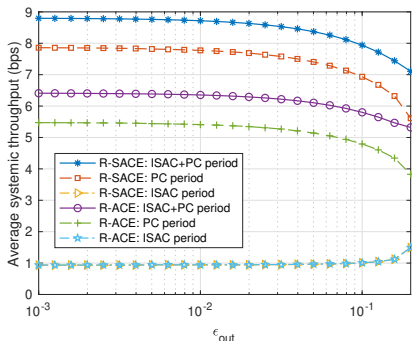


Fig. 9. The AST v.s. ϵ_{out} in R-SACE and R-ACE mechanisms.

communication during the PC period. When the BS detects the presence of TC J , it communicates with CU I and TC J via the direct BS-CU I and BS-TC J links, respectively. To alleviate mutual interference, the communication of CU I is limited by the tolerable interference of TC J . Otherwise, when BS detects the absence of TC J , it communicates only with CU I via the direct BS-CU I link. Therefore, the average outage rate of CU I during the PC period is given by $P_{I(2)}^{(1)} \log_2(1 + \hat{\gamma}_I^{S(1)}) + P_{I(2)}^{(0)} \log_2(1 + \hat{\gamma}_I^{S(0)})$, where $\hat{\gamma}_I^{S(1)} = |\hat{\mathbf{h}}_I^H \mathbf{w}_I|^2 / (|\hat{\mathbf{h}}_I^H \mathbf{w}_J|^2 + \sigma^2)$ and $\hat{\gamma}_I^{S(0)} = |\hat{\mathbf{h}}_I^H \mathbf{w}_I|^2 / \sigma^2$. The average data rate of the present TC J during the PC period is given by $P_J^{(1)} \log_2(1 + \hat{\gamma}_J^{S(1)})$, where $\hat{\gamma}_J^{S(1)} = \frac{|\hat{\mathbf{h}}_J \mathbf{w}_J|^2}{|\hat{\mathbf{h}}_J \mathbf{w}_I|^2 + \sigma^2}$. The interference constraint is $|\hat{\mathbf{h}}_J^H \mathbf{w}_I|^2 \leq \bar{\epsilon}_J$, which is different from C6 in the R-SACE mechanism.

1) *Compare with R-ACE mechanism:* Fig. 9 illustrates the AST varying with ϵ_{out} in the proposed R-SACE mechanism and the baseline R-ACE mechanism. This figure shows that during the ISAC period, the throughput achieved by the R-SACE mechanism is the same as that achieved by the R-ACE mechanism, as shown in Table I. During the PC period, the proposed R-SACE mechanism achieves higher throughput than the R-ACE mechanism. This result is due to the performance-guaranteed sensing result obtained during the ISAC period in the R-SACE mechanism, which aids in better communication coordination between two UEs during the PC period. As a result, the proposed R-SACE mechanism achieves higher throughput in the PC period, which further benefits the higher systemic throughput compared to the R-ACE mechanism.

Fig. 10 illustrates the average throughputs of CU I , TC J , and the entire system changing with the probability P_{J_1} in R-SACE and R-ACE mechanisms. As shown in this figure, the average throughput of CU I decreases with P_{J_1} in both

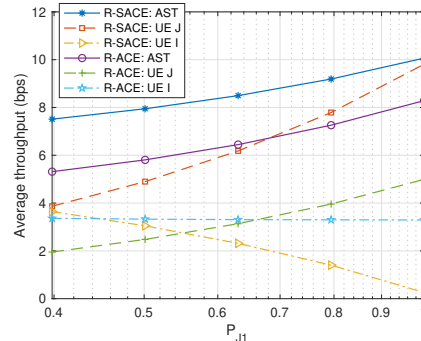


Fig. 10. Average throughput v.s. P_{J_1} in R-SACE and R-ACE mechanisms.

R-SACE and R-ACE mechanisms. This phenomenon occurs because a higher P_{J_1} indicates a higher probability of TC J being present. As a result, the possibility of CU I encountering interference from the BS-TC J link increases, leading to a decrease in the average throughput of CU I . On the other hand, the average throughput of TC J in both R-SACE and R-ACE mechanisms increases with P_{J_1} . This result is obvious, as evidenced by the theoretical expressions of the average data rate of TC J in Table II. Finally, the average throughput of the entire system, i.e., the AST, increases with P_{J_1} because the improvement in the throughput of TC J is greater than the decrease in the throughput of CU I . Furthermore, the proposed R-SACE mechanism achieves a higher AST than the R-ACE mechanism due to the effective assistance of the performance-guaranteed sensing results obtained during the ISAC period.

2) *Comparison with S-ACE mechanism:* Fig. 11 presents the average throughputs of CU I , TC J , and the entire system changing with the BS-CU I distance in R-SACE and S-ACE mechanisms. As shown in this figure, the average throughput of CU I decreases with the distance between BS and CU I . This is because the increasing BS-CU I distance results in more serious large-scale fading on the BS-CU I and BS-RIS-CU I links. On the other hand, the average throughput of TC J slightly increases with the distance between BS and CU I . This is because TC J experiences less interference from the communication links between BS and CU I , as the BS-CU I distance increases. This phenomenon can be further explained by the theoretical expression of SINR of TC J in Eq. (10).

Fig. 11 also shows that the average throughput of CU I in the proposed R-SACE mechanism and the S-ACE mechanism is nearly the same. This result indicates that the RIS in the R-SACE mechanism offers negligible assistance in enhancing the communication performance for CU I in comparison to the

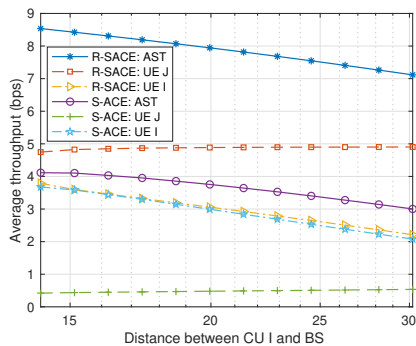


Fig. 11. Average throughput v.s. the distance between CU I and BS.

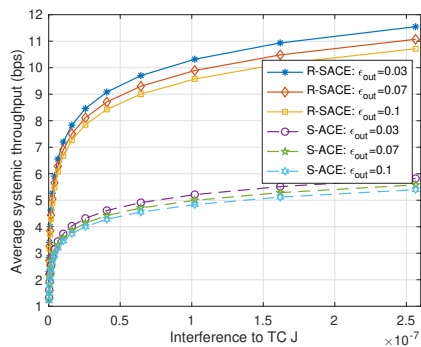


Fig. 12. The AST and interference on TC J changing with ϵ_{out} .

S-ACE mechanism. The reason can be explained as follows. First, when TC J is present during the PC period, the double fading of the RIS-assisted BS-RIS-CU I link degrades the SINR of CU I in the R-SACE mechanism. Alternatively, when TC J is absent during the PC period, RIS contributes little to the increment of SINR of CU I due to the stronger direct BS-CU I link. Therefore, even if CU I achieves additional communication performance during the ISAC period, the RIS-assisted communication performance gain for CU I is insignificant in the R-SACE mechanism when compared to the S-ACE mechanism. For TC J , the RIS in the R-SACE mechanism significantly improves its communication performance when compared to the S-ACE mechanism. This advantage stems from the significantly reduced interference encountered by TC J from CU I with the assistance of RIS during the PC period. The theoretical expressions of $\hat{\gamma}_J^{(l)}$ in Eq. (10) and $\hat{\gamma}_J^{S(l)}$ in Table II further support this result. Finally, the R-SACE mechanism outperforms the S-ACE mechanism in terms of the systemic communication performance, by inheriting the RIS-assisted notable performance enhancement for TC J .

Fig. 12 illustrates the AST and the interference to TC J considering different ϵ_{out} in R-SACE and S-ACE mechanisms. As shown in this figure, the AST in either the R-SACE or the S-ACE mechanism decreases with ϵ_{out} . This phenomenon is consistent with that in Fig. 8 and Fig. 9. Furthermore, this figure shows that the proposed R-SACE mechanism achieves a higher AST than the S-ACE mechanism under the same interference to the TC J . In other words, the TC J experiences more severe interference in the S-ACE mechanism than in the

proposed R-SACE mechanism when the AST is the same. On the other hand, from the CU I perspective, the presence of the RIS allows for a more relaxed constraint under the same interference threshold $\bar{\epsilon}_J$. Specifically, the constraint condition $|\mathbf{g}_{RJ}^H \Theta \mathbf{G} \mathbf{w}_I|^2 \leq \bar{\epsilon}_J$, to the beamforming \mathbf{w}_I is less stringent compared to the interference constraint condition $|\hat{\mathbf{h}}_J^H \mathbf{w}_I|^2 \leq \bar{\epsilon}_J$ in the S-ACE mechanism. This result further demonstrates the effectiveness of RIS in suppressing mutual interference and coordinating communication performance between CU I and TC J .

VI. CONCLUSION

This paper investigated the RIS-assisted sensing-aided communication enhancement (R-SACE) with imperfect CSI. We proposed a new R-SACE model where an ISAC BS provides downlink communication services to both a static communication user and an aperiodically present target that needs to be detected first. The availabilities of either or both the direct link and the RIS-assisted reflected link are considered. Average systemic throughput (AST) was maximized by jointly optimizing the time protocol design, the transmission beamforming of BS, and the phase shift of RIS. The non-convex probabilistic mixed optimization problem was transformed and then solved by the proposed fixed-point iterative (FPI) algorithm. Simulation results verified that the proposed R-SACE mechanism achieved an optimal balance between sensing and communication in functional assistance and competing resources, including both temporal and spatial resources. This optimal balance ultimately enhanced systemic communication performance by at least 21.53% and 75% through the proposed R-SACE mechanism when compared to the R-ACE and S-ACE mechanisms, respectively. The multi-objective optimization problem that optimizes both S&C performances will be further investigated in future work.

APPENDIX A PROOF OF PROPOSITION 1

Given $\hat{d}_l = \frac{\hat{c}_l}{2^{\hat{R}_l} - 1}$, Eq. (14) can be rewritten as

$$\begin{aligned} \Pr \left[d_l \geq \hat{d}_l | \hat{\mathbf{f}}_l \right] &= \Pr \left[d_l \geq \left(\hat{c}_l / (2^{\hat{R}_l} - 1) \right) | \hat{\mathbf{f}}_l \right] \\ &= \Pr \left[\frac{\hat{c}_l}{d_l} \leq 2^{\hat{R}_l} - 1 | \hat{\mathbf{f}}_l \right] \leq \epsilon_{\text{out}}/2. \end{aligned} \quad (46)$$

When $c_l \geq \hat{c}_l$, it's easy to obtain that

$$\Pr \left[\frac{c_l}{d_l} \leq 2^{\hat{R}_l} - 1 | c_l > \hat{c}_l, \hat{\mathbf{f}}_l \right] \leq \epsilon_{\text{out}}/2. \quad (47)$$

Then, according to Eq. (15), we can get

$$\Pr \left[c_l > \hat{c}_l | \hat{\mathbf{f}}_l \right] = 1 - \epsilon_{\text{out}}/2. \quad (48)$$

Since $\Pr\left[\frac{c_l}{d_l} < 2^{\hat{R}_l} - 1 | c_l \leq \hat{c}_l, \hat{\mathbf{f}}_l\right] \leq 1$, by substituting Eqs. (15), (47), and (48) into Eq. (13), we have

$$\begin{aligned} & \Pr\left[\frac{c_l}{d_l} < 2^{\hat{R}_l} - 1 | c_l \leq \hat{c}_l, \hat{\mathbf{f}}_l\right] \cdot \Pr\left[c_l \leq \hat{c}_l | \hat{\mathbf{f}}_l\right] \\ & + \Pr\left[\frac{c_l}{d_l} < 2^{\hat{R}_l} - 1 | c_l > \hat{c}_l, \hat{\mathbf{f}}_l\right] \cdot \Pr\left[c_l > \hat{c}_l | \hat{\mathbf{f}}_l\right] \quad (49) \\ & \leq \epsilon_{\text{out}}/2 + \epsilon_{\text{out}}/2(1 - \epsilon_{\text{out}}/2) \\ & = \epsilon_{\text{out}} - \epsilon_{\text{out}}^2/4 \approx \epsilon_{\text{out}}, \end{aligned}$$

for $\epsilon_{\text{out}} \ll 1$. As a conclusion, the constraint C_1 can be rewritten as Eqs. (14) and (15).

APPENDIX B PROOF OF PROPOSITION 3

When τ_1 is fixed, $\rho_0 \tilde{R}_0$ is a constant term in problem **P2**. Thus, the joint optimization of Θ , \mathbf{w}_I , \mathbf{w}_J can be recast as

$$\begin{aligned} \max_{\Theta, \mathbf{w}_I, \mathbf{w}_J} \tilde{O}_T &= \sum_{l=1}^3 \rho_l \tilde{R}_l = \sum_{l=1}^3 \rho_l \log_2(1 + \tilde{\gamma}_l) \quad (50) \\ &= \rho_1 \log_2(1 + \tilde{\gamma}_1(\Theta, \mathbf{w}_I, \mathbf{w}_J)) \\ &+ \rho_2 \log_2(1 + \tilde{\gamma}_2(\Theta, \mathbf{w}_I)) \\ &+ \rho_3 \log_2(1 + \tilde{\gamma}_3(\Theta, \mathbf{w}_I, \mathbf{w}_J)) \\ \text{s.t. } &C4 - C6. \end{aligned}$$

Let $\tilde{\gamma}_{21} = \frac{\mathcal{F}^{-1}(\frac{\epsilon_{\text{out}}}{2}) L_I^2 \|\mathbf{w}_I\|^2}{\sigma_I^2}$, $\tilde{\gamma}_{22} = \frac{|\mathbf{g}_{RI}^H \Theta \mathbf{G} \mathbf{w}_I|^2}{\sigma_I^2}$. We define $\tilde{R}'_2 = \rho_2 \log_2(1 + \tilde{\gamma}_{21}(\mathbf{w}_I)) + \rho_2 \log_2(1 + \tilde{\gamma}_{22}(\Theta, \mathbf{w}_I))$. Then, by solving the functions of first-order derivatives $\partial \tilde{R}'_2 / \partial \Theta = 0$ and $\partial \tilde{R}'_2 / \partial \mathbf{w}_I = 0$, we get that \tilde{R}'_2 and \tilde{R}_2 keep the same tendency changing with Θ and meanwhile have the same extreme point within the feasible region of Θ . As a result, the optimizations of Θ , \mathbf{w}_I , \mathbf{w}_J in Eq. (50) is equivalent to

$$\begin{aligned} \max_{\Theta, \mathbf{w}_I, \mathbf{w}_J} \tilde{O}_T &= \sum_{m=1}^4 \rho_m \log_2(1 + \tilde{\gamma}'_m) \quad (51) \\ &= \rho_1 \log_2(1 + \tilde{\gamma}'_1(\Theta, \mathbf{w}_I, \mathbf{w}_J)) \\ &+ \rho_2 \log_2(1 + \tilde{\gamma}'_2(\mathbf{w}_I)) \\ &+ \rho_3 \log_2(1 + \tilde{\gamma}'_3(\Theta, \mathbf{w}_I, \mathbf{w}_J)) \\ &+ \rho_4 \log_2(1 + \tilde{\gamma}'_4(\Theta, \mathbf{w}_I)) \\ \text{s.t. } &C4 - C6, \end{aligned}$$

$$\text{where } \rho_4 = \rho_2 \text{ and } \tilde{\gamma}'_m = \begin{cases} \tilde{\gamma}_1, & m = 1 \\ \tilde{\gamma}_{21}, & m = 2 \\ \tilde{\gamma}_3, & m = 3 \\ \tilde{\gamma}_{22}, & m = 4. \end{cases}$$

Next, we utilize the Lagrangian dual transform method to recast the sum-of-logarithm problem in Eq. (51) as a sum-of-ratio problem. According to Theorems 3 and 4 in [35], we introduce an auxiliary vector $\mathbf{v} = [v_1, v_2, v_3, v_4]$ and thus the sum-of-logarithm objective function can be recast as

$$\sum_{m=1}^4 \rho_m \log_2(1 + v_m) - \rho_m v_m + \sum_{m=1}^4 \rho_m (1 + v_m) \tilde{\gamma}'_m. \quad (52)$$

We rewrite $\sum_{m=1}^4 \rho_m (1 + v_m) \tilde{\gamma}'_m$ as $\sum_{m=1}^4 \rho_m (1 + v_m) \frac{\tilde{\gamma}'_m}{\tilde{\gamma}'_m}$.

Then, we utilize the QT method [34] to recast the sum-of-ratio fractional programming problem. Specifically, we introduce two auxiliary complex vectors $\mathbf{u} = [u_1, u_4]$ and $\mathbf{y} = [\mathbf{y}_2, \mathbf{y}_3]$, where u_1 and u_4 are two complex variables and $\mathbf{y}_2 \in \mathbb{C}^{K \times 1}$ and $\mathbf{y}_3 \in \mathbb{C}^{K \times 1}$ are two complex vectors. Following that, the numerator functions in $\rho_m (1 + v_m) \frac{\tilde{\gamma}'_m}{\tilde{\gamma}'_m}$, $\forall m$ can be recast as

$$\rho_m (1 + v_m) \tilde{\gamma}'_m \Rightarrow \begin{cases} 2\sqrt{\rho_1(1+v_1)\epsilon_{\text{out}} \text{Re}\{u_1^H \mathbf{g}_{RI}^H \Theta \mathbf{G} \mathbf{w}_I\}}, & m = 1, \\ 2\sqrt{\rho_2(1+v_2) \mathcal{F}^{-1}(\frac{\epsilon_{\text{out}}}{2}) L_I^2 \text{Re}\{\mathbf{y}_2^H \mathbf{w}_I\}}, & m = 2, \\ 2\sqrt{\rho_3(1+v_3) \mathcal{F}^{-1}(\frac{\epsilon_{\text{out}}}{2}) L_J^2 \text{Re}\{\mathbf{y}_3^H \mathbf{w}_J\}}, & m = 3, \\ 2\sqrt{\rho_4(1+v_4) \text{Re}\{u_4^H \mathbf{g}_{RI}^H \Theta \mathbf{G} \mathbf{w}_I\}}, & m = 4. \end{cases} \quad (53)$$

The denominator functions in $\rho_m (1 + v_m) \frac{\tilde{\gamma}'_m}{\tilde{\gamma}'_m}$, $\forall m$ can be recast as

$$\tilde{\gamma}'_m \Rightarrow \begin{cases} -|u_1|^2 (2L_I^2 (\|\hat{\mathbf{f}}_I\|^2 + \|\mathbf{1}_K\|^2 \sigma_e^2) \|\mathbf{w}_J\|^2 + \epsilon_{\text{out}} \sigma_I^2), & m = 1, \\ -\|\mathbf{y}_2\|^2 \sigma_I^2, & m = 2, \\ -\|\mathbf{y}_3\|^2 (|\mathbf{g}_{RJ}^H \Theta \mathbf{G} \mathbf{w}_I|^2 + \sigma_J^2), & m = 3, \\ -|u_4|^2 \sigma_I^2, & m = 4. \end{cases} \quad (54)$$

Finally, by substituting (53) and (54) into (52), the objective function in Eq. (51) can be recast as the transformed objective function in Eq. (34). Last but not the least, the consistencies between the original problem and the QT-based transformed problem in both the optimal solutions and the optimal value of the objective function are demonstrated in [34] and [35].

REFERENCES

- [1] Z. Wei, F. Liu, C. Masouros, N. Su, and A. P. Petropulu, "Toward multi-functional 6G wireless networks: Integrating sensing, communication, and security," *IEEE Commun. Mag.*, vol. 60, no. 4, pp. 65–71, Apr. 2022.
- [2] J. A. Zhang et al., "Enabling joint communication and radar sensing in mobile networks—A survey," *IEEE Commun. Surveys Tuts.*, vol. 24, no. 1, pp. 306–345, 1st Quart. 2022.
- [3] H. Zhang, "Joint Waveform and Phase Shift Design for RIS-Assisted Integrated Sensing and Communication Based on Mutual Information," *IEEE Commun. Lett.*, vol. 26, no. 10, pp. 2317–2321, Oct. 2022.
- [4] F. Liu et al., "Integrated Sensing and Communications: Toward Dual-Functional Wireless Networks for 6G and Beyond," *IEEE J. Sel. Area Commun.*, vol. 40, no. 6, pp. 1728–1767, June 2022.
- [5] F. Dong, F. Liu, Y. Cui, W. Wang, K. Han and Z. Wang, "Sensing as a Service in 6G Perceptive Networks: A Unified Framework for ISAC Resource Allocation," *IEEE Trans. Wirel. Commun.*, vol. 22, no. 5, pp. 3522–3536, May 2023.
- [6] R. Liu, M. Li, H. Luo, Q. Liu and A. L. Swindlehurst, "Integrated Sensing and Communication with Reconfigurable Intelligent Surfaces: Opportunities, Applications, and Future Directions," *IEEE Wirel. Commun.*, vol. 30, no. 1, pp. 50–57, Feb. 2023.
- [7] Z. Zhang et al., "Active RIS vs. Passive RIS: Which Will Prevail in 6G?," *IEEE Trans. Commun.*, vol. 71, no. 3, pp. 1707–1725, March 2023.
- [8] Y. Lin, S. Jin, M. Matthaiou and X. You, "Tensor-Based Algebraic Channel Estimation for Hybrid IRS-Assisted MIMO-OFDM," *IEEE Transactions on Wireless Communications*, vol. 20, no. 6, pp. 3770–3784, June 2021.
- [9] X. Mu, Y. Liu, L. Guo, J. Lin and R. Schober, "Simultaneously Transmitting and Reflecting (STAR) RIS Aided Wireless Communications," *IEEE Trans. Wirel. Commun.*, vol. 21, no. 5, pp. 3083–3098, May 2022.
- [10] E. Shtaiwi, H. Zhang, A. Abdelhadi, A. Lee Swindlehurst, Z. Han and H. Vincent Poor, "Sum-rate Maximization for RIS-assisted Integrated Sensing and Communication Systems with Manifold Optimization," *IEEE Trans. Commun.*, vol. 71, no. 8, pp. 4909–4923, Aug. 2023.

- [11] R. Liu, M. Li, Q. Liu and A. L. Swindlehurst, "SNR/CRB-Constrained Joint Beamforming and Reflection Designs for RIS-ISAC Systems," *IEEE Trans. Wirel. Commun.*, vol. 23, no. 7, pp. 7456-7470, July 2024.
- [12] A. A. Salem, M. H. Ismail and A. S. Ibrahim, "Active Reconfigurable Intelligent Surface-Assisted MISO Integrated Sensing and Communication Systems for Secure Operation," *IEEE Trans. Vehi. Technol.*, vol. 72, no. 4, pp. 4919-4931, April 2023.
- [13] Z. Xing, R. Wang and X. Yuan, "Joint Active and Passive Beamforming Design for Reconfigurable Intelligent Surface Enabled Integrated Sensing and Communication," *IEEE Trans. Commun.*, vol. 71, no. 4, pp. 2457-2474, Apr. 2023.
- [14] M. Luan, B. Wang, Z. Chang, T. Hämäläinen and F. Hu, "Robust Beamforming Design for RIS-Aided Integrated Sensing and Communication System," *IEEE Trans. Intelligent Transportation Systems*, vol. 24, no. 6, pp. 6227-6243, June 2023.
- [15] M. Hua, Q. Wu, W. Chen, O. A. Dobre and A. L. Swindlehurst, "Secure Intelligent Reflecting Surface-Aided Integrated Sensing and Communication," *IEEE Trans. Wirel. Commun.*, vol. 23, no. 1, pp. 575-591, Jan. 2024.
- [16] Q. Zhu, M. Li, R. Liu and Q. Liu, "Joint Transceiver Beamforming and Reflecting Design for Active RIS-Aided ISAC Systems," *IEEE Trans. Veh. Technol.*, vol. 72, no. 7, pp. 9636-9640, July 2023.
- [17] Z. Liu, X. Li, H. Ji, H. Zhang and V. C. M. Leung, "Toward STAR-RIS-Empowered Integrated Sensing and Communications: Joint Active and Passive Beamforming Design," *IEEE Trans. Vehi. Technol.*, vol. 72, no. 12, pp. 15991-16005, Dec. 2023.
- [18] Z. Yu et al., "Active RIS-Aided ISAC Systems: Beamforming Design and Performance Analysis," *IEEE Trans. Commun.*, vol. 72, no. 3, pp. 1578-1595, March 2024.
- [19] N. González-Prelcic et al., "The Integrated Sensing and Communication Revolution for 6G: Vision, Techniques, and Applications," in *Proceedings of the IEEE*, doi: 10.1109/JPROC.2024.3397609.
- [20] C. Liu, X. Hu, M. Peng and C. Zhong, "Sensing for Beamforming: An IRS-Enabled Integrated Sensing and Communication Framework," 2022 IEEE International Conference on Communications (ICC), Seoul, Korea, Republic of, 2022, pp. 5567-5572.
- [21] Z. Yu, X. Hu, C. Liu, M. Peng and C. Zhong, "Location Sensing and Beamforming Design for IRS-Enabled Multi-User ISAC Systems," *IEEE Trans. Signal Process.*, vol. 70, pp. 5178-5193, 2022.
- [22] Y. Liu, L. Wu, Z. Zhang, J. Dang and B. Zhu, "Space-Time Coding Design for RIS-Assisted Integrated Sensing and Communication System," *IEEE Wirel. Commun. Lett.*, vol. 13, no. 7, pp. 1943-1947, July 2024.
- [23] X. Li, Y. Chen, H. Wang and S. Sheng, "R-SACE: RIS-Enabled Sensing-Aided Communication Enhancement in ISAC Systems," 2023 IEEE 22nd International Conference on Trust, Security and Privacy in Computing and Communications (TrustCom), Exeter, United Kingdom, 2023, pp. 2714-2719.
- [24] X. Li, H. Wang, Y. Chen and S. Sheng, "Joint Resource Allocation and Reflecting Precoding Design for RIS-Assisted ISAC Systems," *IEEE Wirel. Commun. Lett.*, vol. 13, no. 4, pp. 1193-1197, April 2024.
- [25] Z. -M. Jiang et al., "Intelligent Reflecting Surface Aided Dual-Function Radar and Communication System," *IEEE Systems J.*, vol. 16, no. 1, pp. 475-486, Mar 2022.
- [26] H. Zhang, "Joint Waveform and Phase Shift Design for RIS-Assisted Integrated Sensing and Communication Based on Mutual Information," *IEEE Commun. Lett.*, vol. 26, no. 10, pp. 2317-2321, Oct. 2022.
- [27] E. Shtaiwi et al., "Channel estimation approach for RIS assisted MIMO systems," *IEEE Trans. Cognit. Commun. Netw.*, vol. 7, no. 2, pp. 452-465, Jun. 2021.
- [28] S. M. Kay, "Fundamentals of Statistical Signal Processing: Detection Theory", vol. 2. Englewood Cliffs, NJ, USA: Prentice-Hall, 1993.
- [29] Z.-Q. He and X. Yuan, "Cascaded channel estimation for large intelligent metasurface assisted massive MIMO," *IEEE Wireless Commun. Lett.*, vol. 9, no. 2, pp. 210-214, Feb. 2020.
- [30] C. You, B. Zheng, and R. Zhang, "Channel estimation and passive beamforming for intelligent reflecting surface: Discrete phase shift and progressive refinement," *IEEE J. Sel. Areas Commun.*, vol. 38, no. 11, pp. 2604-2620, Nov. 2020.
- [31] D. W. K. Ng, E. S. Lo, and R. Schober, "Energy-efficient resource allocation in OFDMA systems with large numbers of base station antennas," *IEEE Trans. Wireless Commun.*, vol. 11, no. 9, pp. 3292-3304, Sep. 2012.
- [32] X. Wang, F.-C. Zheng, P. Zhu, and X. You, "Energy-efficient resource allocation in coordinated downlink multicell OFDMA systems," *IEEE Trans. Veh. Technol.*, vol. 65, no. 3, pp. 1395-1408, Mar. 2016.
- [33] F. Fang, H. Zhang, J. Cheng, S. Roy and V. C. M. Leung, "Joint User Scheduling and Power Allocation Optimization for Energy-Efficient NOMA Systems With Imperfect CSI," *IEEE J. Sel. Areas Commun.*, vol. 35, no. 12, pp. 2874-2885, Dec. 2017.
- [34] K. Shen and W. Yu, "Fractional programming for communication systems—Part I: Power control and beamforming," *IEEE Trans. Signal Process.*, vol. 66, no. 10, pp. 2616-2630, May 2018.
- [35] K. Shen and W. Yu, "Fractional Programming for Communication Systems—Part II: Uplink Scheduling via Matching," *IEEE Trans. Signal Process.*, vol. 66, no. 10, pp. 2631-2644, May 2018.
- [36] H. Luo, R. Liu, M. Li, Y. Liu and Q. Liu, "Joint Beamforming Design for RIS-Assisted Integrated Sensing and Communication Systems," *IEEE Trans. Veh. Technol.*, vol. 71, no. 12, pp. 13393-13397, Dec. 2022.
- [37] D. Kudathanthirige, D. Gunasinghe and G. Amarasinghiya, "Performance Analysis of Intelligent Reflective Surfaces for Wireless Communication," 2020 IEEE International Conference on Communications (ICC), Dublin, Ireland, 2020, pp. 1-6.
- [38] J. Gu, G. Ge, H. Wang, Y. Xu and G. Ding, "Beamforming Design for Integrated Communication and Jamming Systems Under Imperfect CSI," 2023 International Conference on Ubiquitous Communication (Ucom), Xi'an, China, 2023, pp. 269-274.
- [39] C. Vlădeanu, O. M. K. Al-Dulaimi, A. Marțian and D. C. Popescu, "Average Energy Detection With Adaptive Threshold for Spectrum Sensing in Cognitive Radio Systems," *IEEE Transactions on Vehicular Technology*, vol. 73, no. 11, pp. 17222-17230, Nov. 2024.

Xiaohui Li received the Ph.D. degree in communication and information system from the Key Wireless Laboratory of Jiangsu Province, the School of Telecommunication and Information Engineering, Nanjing University of Posts and Telecommunications (NUPT), Nanjing, China. She was a Visiting Student at the Department of Electrical and Computer Engineering, Western University, London, Canada, in 2018. She is currently a lecturer with the School of Telecommunication and Information Engineering, NUPT, Nanjing, China. Her current research interests include Internet of Things, crowd sensing, incentive mechanism, and dynamic spectrum access and sharing.

Qi Zhu received the bachelor's and master's degrees in radio engineering from the Nanjing University of Posts and Telecommunications (NUPT), Nanjing, China, in 1986 and 1989, respectively. She is currently a Professor with the School of Telecommunication and Information Engineering, NUPT, Nanjing, China. Her research interests include technology of next-generation communication, broadband wireless access, orthogonal frequency division multiplexing, and dynamic allocation of radio resources.

Yunpei Chen received the Ph.D. degree in communication and information systems from Nanjing University of Posts and Telecommunications, Nanjing, China, in 2023. His research interests are in the areas of next-generation broadband networks and wireless communication systems, with an emphasis on analysis of Non-Orthogonal Multiple Access (NOMA) and stochastic geometry applied to wireless systems.

Chadi Assi received the M.A.Sc. and Ph.D. degrees from the Graduate Center, City University of New York. He is a Professor with the Concordia Institute for Information Systems Engineering, Concordia University, Montreal, Canada, where he currently holds a Tier I University Research Chair. Before joining Concordia University in 2003, he was a Visiting Scientist with Nokia Research Center, Boston, from 2002 to 2003, working on quality-of-service in optical access networks. His current research interests are in the general areas of Networks (wired and cellular), network design and modeling, network optimization, and cyber security. He received the prestigious Mina Rees Dissertation Award from the City University of New York in August 2002 for his research on wavelength-division-multiplexing optical networks and lightpath provisioning. He served on the editorial board of several IEEE journals and is currently serving as an Associate Editor for the IEEE TRANSACTIONS ON VEHICULAR TECHNOLOGY, IEEE TRANSACTIONS ON MOBILE COMPUTING, and IEEE TRANSACTIONS ON NETWORK AND SERVICE MANAGEMENT.

Yifei Yuan received Bachelor degree and Master degree from Tsinghua University in China and Ph. D degree from Carnegie Mellon University in USA. He was with Alcatel-Lucent from 2000 to 2008. From 2008 to 2020, he was with ZTE Corporation as a technical director and chief engineer, responsible for standards & research of 4G LTE-Advanced and 5G technologies. He joined the China Mobile Research Institute in 2020 as a Chief Expert, responsible for 6G wireless research. He has extensive publications, including 10 books on LTE-Advanced, 5G and 6G. He has over 60 granted US patents.